IκB kinase, p38 MAPK, and Akt are major signaling molecules thought to play a pivotal role in most types of cytokine production in various cells (Hiscott et al., 2001; Adcock et al., 2006). Single strand RNA such as viral RNA binds and activates helicase, which further activates IκB kinase pathways, resulting in the production of certain types of cytokine (Lee and Lau, 2007). In addition, it is well known that phosphorylation of p38 MAPK is associated with the production of cytokines in many types of cells (Suzuki et al., 1999; Wong et al., 2005). Thus, these signaling molecules may be associated with the production of cytokines in virus-infected cells, although the details are not as yet known.

Human lung fibroblasts are reported to be susceptible to various respiratory viruses such as PIV and RV (Bousse et al., 2006; Jang et al., 2009). In addition, lung fibroblasts may be associated with remodeling involved in fibrosis in the small airways (Puxeddu et al., 2006). In asthmatics, viral infections are more likely to result in lower respiratory tract infection (Gern, 2009), and moreover, these infections are not restricted to the respiratory epithelium, but can spread to the structural cells such as smooth muscle cells and fibroblasts (Holgate et al., 2004b). From these background, in the present study we chose human fetal lung fibroblasts to examine the cytokine milieu of the asthmatic airway under chronic viral infection. We hypothesized that PIV infection might induce virus-induced asthma-related cytokine production in fetal lung fibroblasts. To explore this possibility, we profiled cytokines released from PIV-infected fetal lung fibroblasts and examined the role of the signaling pathways (IκB kinase, p38 MAPK, and Akt).

MATERIALS AND METHODS
CELLS AND CELL CULTURE

Human fetal lung fibroblasts (MRC-5 cells) were purchased from the American Type Culture Collection (ATCC, Manassas, VA, USA). Cells were grown in 75-cm^2 tissue culture flasks and maintained in Eagle's minimum essential medium (MEM; Invitrogen Life Technologies, CA, USA) containing 10% fetal bovine serum (FBS), L-glutamine (0.6 mg/ml), and 0.35% $NaHCO_3$ at 36°C in a humidified atmosphere containing 5% CO_2 (de Oña et al., 1995).

VIRAL PROPAGATION AND MEASUREMENT OF VIRAL TITERS

Human PIV type 3 (C 243 strain) were obtained from American Tissue Culture Corrections (Rockville, MD, USA) and propagated in Vero E6 cells. When the PIV-infected Vero E6 cells showed cytopathic effects (CPE), they were centrifuged at 4200 × g for 30 min at 4°C to remove debris. To purify the viruses, the supernatants were layered over 50% sucrose in PBS, then centrifuged at 65,000 × g for 2 h at 4°C as previously described (Ueba, 1978). Aliquots of the viruses were stored at −80°C until required.

MEASUREMENT OF CYTOKINE CONCENTRATIONS

We inoculated 0 (no virus) or 1.0 MOI of each virus suspension (100 μl) in Opti-MEM I to the human fetal lung fibroblasts grown in 96-well microplates. Concentrations of cytokines, chemokines, and growth factors in the culture supernatants from each experimental system (virus-infected, UV-inactivated virus, inhibitor-added, and no virus) were obtained at 24 h. To remove the effect of intracellular cytokines/chemokines, we centrifuged the microplates at 1660 × g for 10 min before carefully harvesting the supernatants.

We measured the following 27 cytokines using an available kit (Cytokine assay 27-Plex Panel kit, Bio-Rad, Hercules, CA, USA): interleukins (IL)-1β, 1ra, 2, 4, 5, 6, 7, 8, 9, 10, 12, 13, 15, and 17, interferon (IFN)-γ, granulocyte colony-stimulating factor (G-CSF), granulocyte–macrophage colony-stimulating factor (GM-CSF), tumor necrosis factor (TNF)-α, monocyte chemoattractant protein (MCP)-1, macrophage inflammatory protein (MIP)-1α, 1β, interferon-inducible protein (IP)-10, eotaxin, fibroblast growth factor (FGF) basic, platelet-derived growth factor (PDGF)-bb, regulated on activation normal T-cell expressed and secreted (RANTES), and vascular endothelial growth factor (VEGF). Assays were performed using the Bio-Plex suspension array system according to the manufacturer's instructions (Bio-Rad). Data were automatically processed and analyzed using Bio-Plex Manager Software 5.0 with the standard curve produced from the recombinant cytokine standard. The sensitivity limits for each cytokine were set at 0.1–3 pg/ml (Okazaki et al., 2008; Yoshizumi et al., 2008).

MEASUREMENT OF PHOSPHORYLATION INHIBITION OF IκB KINASE, p38 MAPK, AND Akt

The inhibitors BMS-345541 (4(2′-aminoethyl)amino-1,8-dimethylimidazo(1,2-a)quinoxaline), a specific inhibitor of IκB kinase), SB203580 (4-(4-fluorophenyl)-2-(4-methylsulfinylphenyl)-5-(4-pyridyl)1H-imidazole, a specific inhibitor of p38 MAPK), and Akt inhibitor X (10-(4-(N-diethylamino)butyl)-2-chlorophenoxazine, HCl) were purchased from Calbiochem (KGaA, Darmstadt, Germany). These compounds were dissolved in DMSO (10 mM) and stored at −80°C until required. The optimal concentration of each of these specific inhibitors of signaling protein phosphorylation was preliminary examined, and 10 μM of each inhibitor was found to be suitable for significant inhibition of the phosphorylation of the kinases, results which are compatible with previous reports (MacMaster et al., 2003; Thimmaiah et al., 2005; Zaheer et al., 2009). Phosphorylation of signal molecules induced by PIV was also assessed using a Bio-Plex suspension array system.

STATISTICAL ANALYSIS

Data are expressed as means ± SE. Statistical analyses of cytokine/chemokine concentrations were performed using the Kruskal–Wallis and Mann–Whitney U methods. Subsequent post hoc analysis was conducted using the Bonferroni-adjusted α method. All statistical analyses were performed using SPSS version 12.0 (SPSS Inc., Chicago, IL, USA). Values of $p < 0.05$ were considered significant.

RESULTS
EXPERIMENTAL CONDITIONS

To confirm the infection of human fetal lung fibroblasts with PIV, morphological changes in the cells were examined by light microscopy after 6, 24, and 48 h. No changes were observed 6 h after PIV infection, whereas the cells clearly showed CPE after 48 h of PIV infection (data not shown). We confirmed that there were no significant differences in the amounts of cytokines released between the UV-treated virus treatment, medium with 0.1% DMSO, and medium alone (without the addition of viruses) (data not shown). Of the 27 cytokines examined, significantly higher amounts of 18

cytokines were released after addition of 1.0 MOI of PIV compared with no addition of viruses (data not shown). Cytokine release by viruses was MOI-dependent (data not shown).

CATEGORIZATION OF CYTOKINES RELEASED BY PIV-INFECTED HUMAN FETAL LUNG FIBROBLASTS

Next, we compared the cytokine levels induced between control and PIV-infected fibroblasts. The amounts of 18 cytokines induced by PIV infection were significantly higher, at least at one time point, than those of control cells. The 18 cytokines were categorized into nine groups (Barnes, 2008): proinflammatory cytokines (**Figures 1A–C**), anti-inflammatory cytokines, (**Figure 1D**), Th1 cytokines (**Figures 1E,F**), Th2 cytokines (**Figures 1G–I**),

granulopoiesis-inducing cytokines (**Figures 1J,K**), neutrophil recruitment-inducing chemokines (**Figures 1L,M**), eosinophil recruitment-inducing chemokines (**Figures 1N,O**), and tissue remodeling-related cytokines (**Figures 1P,Q**).

COMPARISON OF PROINFLAMMATORY AND ANTI-INFLAMMATORY CYTOKINES RELEASED BY PIV-INFECTED HUMAN FETAL LUNG FIBROBLASTS

As shown in **Figures 1A–C**, proinflammatory cytokine (IL-1β, IL-6 and TNF-α levels at 24 h after infection with PIV were significantly higher than levels of control cells. Similarly, the level of IL-1ra (anti-inflammatory cytokine) was significantly higher from PIV-infected cells than from the control cells (**Figure 1D**).
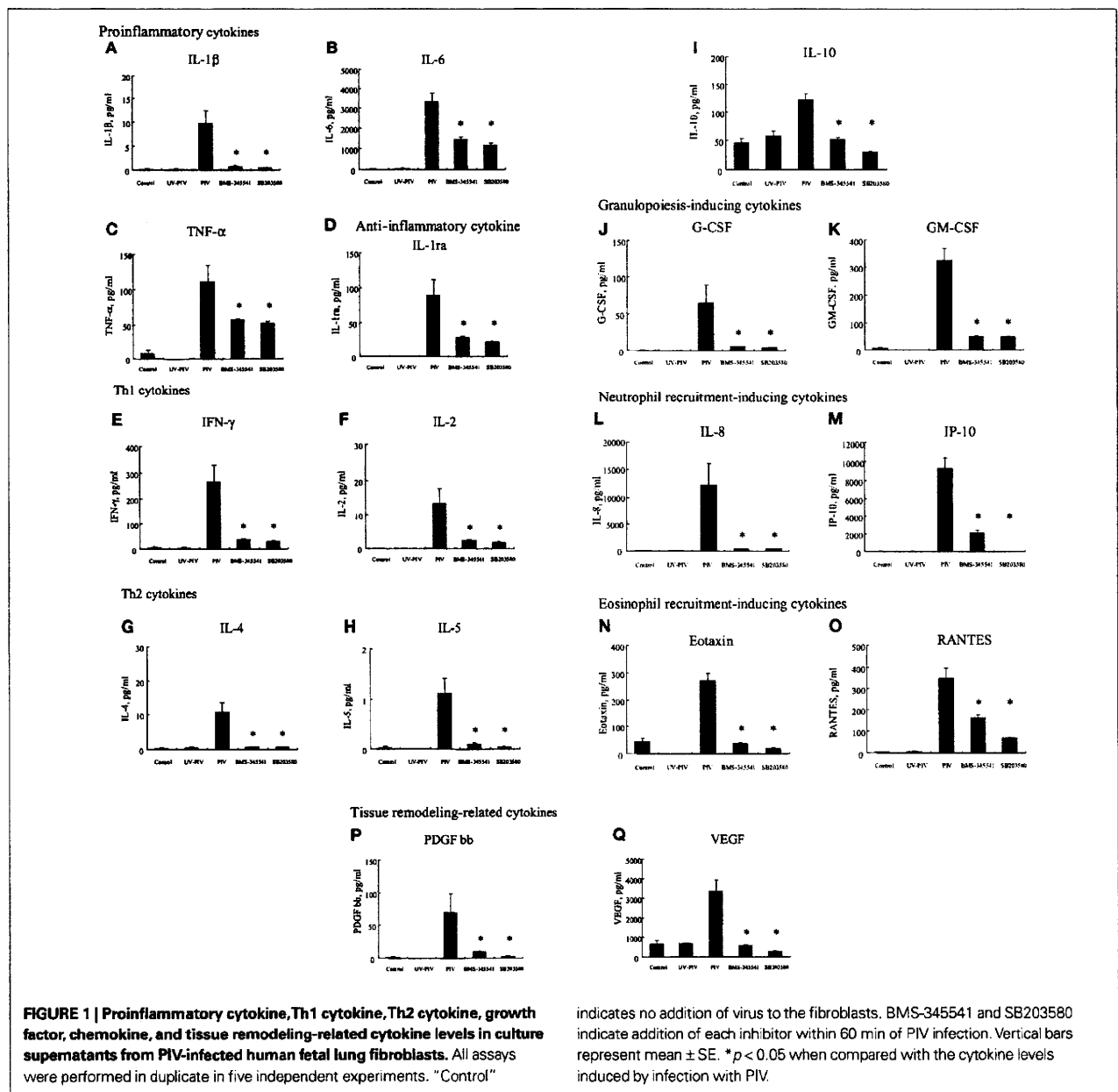
FIGURE 1 | Proinflammatory cytokine, Th1 cytokine, Th2 cytokine, growth factor, chemokine, and tissue remodeling-related cytokine levels in culture supernatants from PIV-infected human fetal lung fibroblasts. All assays were performed in duplicate in five independent experiments. "Control" indicates no addition of virus to the fibroblasts. BMS-345541 and SB203580 indicate addition of each inhibitor within 60 min of PIV infection. Vertical bars represent mean ± SE. *$p < 0.05$ when compared with the cytokine levels induced by infection with PIV.

COMPARISON OF Th1, Th17, AND Th2 CYTOKINES RELEASED BY PIV-INFECTED HUMAN FETAL LUNG FIBROBLASTS

To clarify the differences in Th1, Th17, and Th2 cytokine profiles between PIV-infected human fetal lung fibroblasts and control cells, we compared levels of IFN-γ, IL-2, IL-12, IL-17, IL-4, IL-5, IL-10, and IL-13. We found that small but significant amounts of IFN-γ and IL-2 were produced by PIV-infected fibroblasts compared with control fibroblasts (**Figures 1E,F**), but there was no significant difference in IL-12 levels (data not shown). In addition, PIV infection did not result in any significant difference in amounts of IL-17 from fibroblasts compared with the control (data not shown). PIV infection did result in significantly higher production of IL-4, IL-5, and IL-10 compared with the control (**Figures 1G–I**), but not IL-13 (data not shown).

COMPARISON OF GROWTH FACTORS AND CHEMOKINES RELEASED BY PIV-INFECTED HUMAN FETAL LUNG FIBROBLASTS

G-CSF and GM-CSF levels induced by PIV infection were significantly higher than those induced by the control (**Figures 1J,K**). Similarly, IL-8, IP-10, eotaxin, and RANTES levels were significantly higher in supernatants from PIV-infected fibroblasts than control fibroblasts (**Figures 1L–O**). Regarding cytokines related to tissue remodeling, the same tendency was observed; PDGF-bb and VEGF levels were significantly higher in supernatants from PIV-infected fibroblasts compared with control fibroblasts (**Figures 1P,Q**).
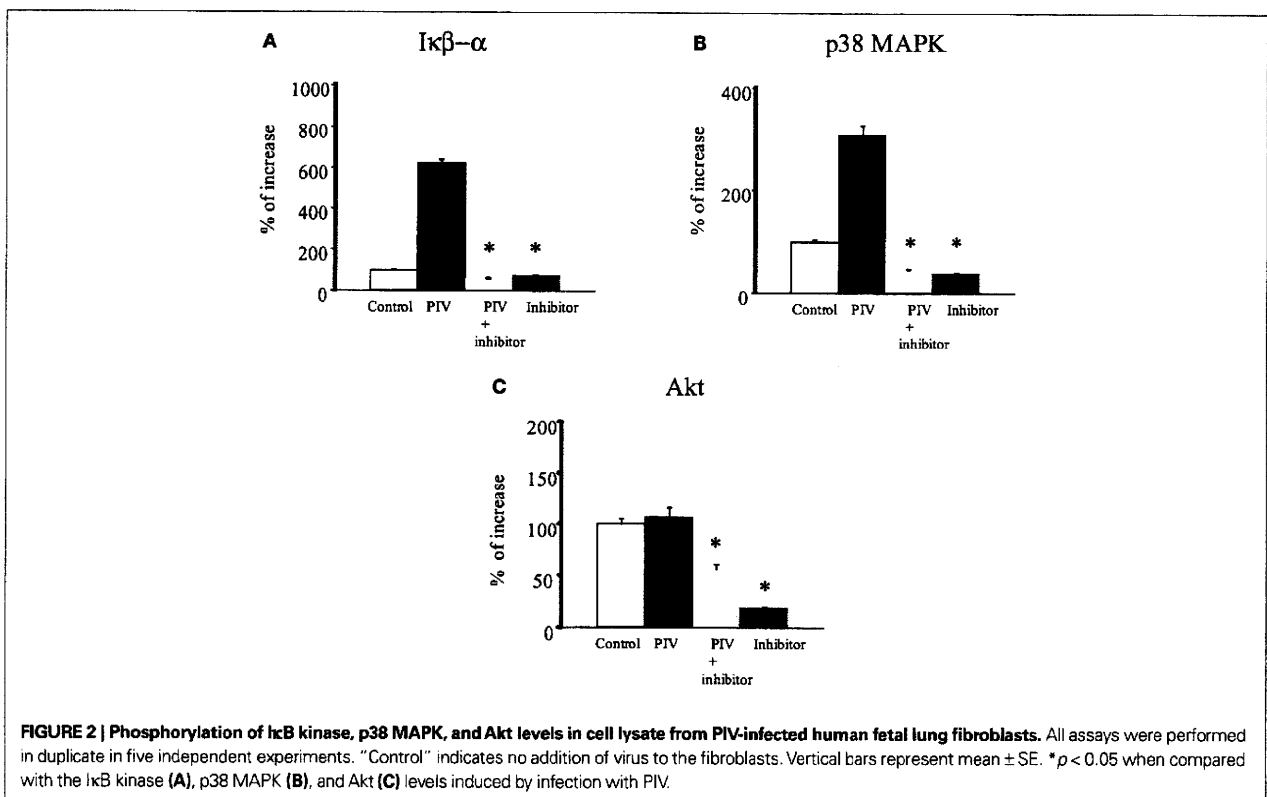
PHOSPHORYLATION OF IκB KINASE, p38 MAPK, AND Akt

To examine possible signal molecules, we investigated the phosphorylation of IκB kinase, p38 MAPK, and Akt. PIV infection dramatically induced the phosphorylation of IκB kinase and p38 MAPK in

MRC-5 cells compared with the control (**Figures 2A,B**). However, no enhancement of Akt phosphorylation was found in the virus-infected cells (**Figure 2C**). Thus, to define the role of the IκB kinase and p38 MAPK pathways in viral induction of cytokines and chemokines, we used their specific inhibitors. As a result, in MRC-5 cells, inhibition of the NF-κB pathway with BMS-345541 (10 μM) significantly inhibited PIV-induced cytokines, namely, IL-1β, 1ra, 2, 4, 5, 6, 8, 10, IFN-γ, TNF-α, G-CSF, GM-CSF, IP-10, eotaxin, RANTES, PDGF-bb, and VEGF (**Figure 1**). Similarly, treatment of the p38 MAPK pathway with SB203580 (10 μM) also significantly inhibited the release of these cytokines (**Figure 1**). The results suggested that both IκB kinase and p38 MAPK phosphorylation was associated with the production and release of various cytokines in the virus-infected cells.

DISCUSSION

We profiled a number of cytokines from PIV-infected fetal lung fibroblasts. Compared with control (no virus) cells, a significant amount of various cytokines were shown to be released, namely, IL-1β, IL-6, TNF-α, IL-1ra, IFN-γ, IL-2, IL-4, IL-5, IL-10, G-CSF, GM-CSF, IL-8, IP-10, eotaxin, RANTES, PDGF-bb, and VEGF. In addition, we found that most aberrantly released cytokines were associated with phosphorylation of IκB kinase and p38 MAPK. Infection by PIV may induce large-scale production of various cytokines in the airway. Although PIV failed to induce IL-12 and IL-17 production, these results indicate that PIV induces a Th2 cytokine milieu as well as eosinophil and neutrophil recruitment to fibroblasts. As a result, Th2 immunity may be augmented, which is likely to be an important mechanism in the pathophysiology of PIV-induced asthma (virus-induced asthma).

FIGURE 2 | Phosphorylation of IκB kinase, p38 MAPK, and Akt levels in cell lysate from PIV-infected human fetal lung fibroblasts. All assays were performed in duplicate in five independent experiments. "Control" indicates no addition of virus to the fibroblasts. Vertical bars represent mean ± SE. *$p < 0.05$ when compared with the IκB kinase **(A)**, p38 MAPK **(B)**, and Akt **(C)** levels induced by infection with PIV.

It is suggested that maximal MAP kinase phosphorylation and activity is seen within 60 min after stimulation. In this study, the phosphorylation of IκB kinase and p38 MAP kinase was examined at 24 h after PIV infection. Thus, it is possible that cytokines produced by PIV-infected MRC-5 cells might be responsible for the induction of MAP kinase phosphorylation, since various cytokines produced after PIV infection have been shown to induce IκB kinase and MAP kinase phosphorylation.

We speculate that the effects of PIV on normal fibroblasts can be extrapolated to corresponding cells in asthmatic airways. Previous studies have shown that increased viral replication and impaired IFN response to viral infection occurs in primary epithelial cells and peripheral blood cells from asthmatics compared with normal subjects (Wark et al., 2005; Contoli et al., 2006; Gehlhar et al., 2006). The increase in virus infection-induced inflammation is a probable explanation for these observations. Asthmatics may also be more susceptible to infection (Holgate, 2007). Furthermore, it has also been suggested that infants who are born with poor antiviral responses and/or airway hyper-responsiveness are prone to repetitive severe illnesses (Gehlhar et al., 2006), and these same abnormalities may increase the risk of recurrent wheezing and possibly asthma. Therefore, fibroblasts from those who develop asthma in earlier childhood might possess a defective IFN response to these respiratory viruses. Such partially defective innate immune responses may result in augmented Th2 immunity in asthmatic patients as well as increased and prolonged airway inflammation (Barrett and Austen, 2009).

A direct causative role for these respiratory viruses in the development of asthma has not been proven yet. Lemanske et al. (2005) suggested at least two potential mechanisms for the development of recurrent wheezing in early childhood. First, healthy infants who undergo repetitive severe viral respiratory infections could develop recurrent wheezing because of lung damage and/or airway remodeling. Second, as mentioned above, infants who are born with weak antiviral responses and/or airway hyper-responsiveness are prone to repetitive severe illnesses, which may increase the risk of recurrent wheezing and possibly asthma. A recent study suggests that RSV-induced wheezing is an indicator of genetic predisposition to asthma, but is not associated with allergic sensitization, irrespective of the family history of asthma (Singh et al., 2007). In the present study, PIV-infected human lung fibroblasts produced and released tissue remodeling-related cytokines (PDGF and VEGF) and proinflammatory cytokines (IL-1β, IL-6, and TNF-α) compared with the control. Using animal models, it was also recently suggested that endotracheal inoculation of PIV induces biological and histological changes reminiscent of asthma (Pelaia et al., 2006). In particular, PIV infection elicits an airway influx of inflammatory cells, bronchial hyper-responsiveness, epithelial damage, and bronchiolar fibrosis (Pelaia et al., 2006). These findings suggest that the recurrence of PIV infections in patients with asthma may contribute to prolonged airway inflammation and airway structural changes typical of the disease (Pelaia et al., 2006). Moreover, our results suggest that PIV-induced tissue remodeling-related cytokines and proinflammatory cytokines from human fibroblasts may be associated with respiratory remodeling and prolonged airway inflammation after infection. Human asthma subjects have exhibited significant increases in IFN-γ, in the supernatants of cultured

bronchoalveolar cells (Krug et al., 1996). Recently, Magnan et al. (2000) demonstrated increased IFN-γ-producing CD8⁺ T cells in asthmatic airways, and the levels of IFN-γ correlated with asthma severity, bronchial hyper-responsiveness, and blood eosinophilia (Ishihara et al., 1997). IFN-γ has been reported to be associated with severe and chronic asthma. In the present study, PIV-infected human lung fibroblasts produced and released IFN-γ, which might be associated with severity of asthma.

Cytokine production-related signaling pathways related to viral infections have been reported (Santoro et al., 2003; Kohlmeier et al., 2009; Zaheer et al., 2009). For example, Lee et al. suggested that single strand viral RNA of influenza virus binds to the host cellular helicase resulting in activation of signaling pathways including IκB kinase (Lee and Lau, 2007). In addition, viral single strand or double strand RNA/MKK3/6 complex can also activate p38 MAPK (Stephan, 2007). Finally, activation of these pathways may lead to the production and release of cytokines in virus-infected cells as an antiviral response (Stephan, 2007). In the present study, at 24 h after PIV infection, phosphorylation of IκB kinase and p38 MAPK and the release of cytokines were significantly increased in lung fibroblasts. Furthermore, inhibition of phosphorylation of these kinases by specific inhibitors significantly eliminated release of cytokines (**Figure 2**). At 24 h after infection, PIV genomes (also single strand RNA) may be significantly propagated (De et al., 1990). A possible reason for this is that the increase in phosphorylation of IκB kinase and p38 MAPK after PIV infection might be associated with propagated PIV genomes in the cells, although we did not observe an increase in the PIV genome/helicase or PIV genome MKK3/6 complex.

Fibroblasts have the potential to play a critical role in remodeling of and changes in the airway matrix (Holgate et al., 2004a). In this study, we found that PIV infection-induced significantly higher production of Th1 and Th2 cytokines from fibroblasts compared to control cells. PIV might promote release of not only inflammatory cytokines but also allergy-related cytokines in virus-infected MRC-5 cells. From the present results and previous our results suggest that aberrant release/production of various cytokines (i.e., cytokine storm) due to PIV or RSV infection is also associated with severe respiratory infection such as pneumonia (Ishioka et al., 2010). In addition, we showed that this cytokine production may be closely linked to phosphorylation of signal molecules such as IκB kinase and p38 MAPK. Recurrent RSV infection may damage the lower respiratory airways and induce remodeling. Finally, our findings suggest that PIV infection-induced aberrant phosphorylation of IκB kinase and p38 MAPK in lung fibroblasts might mediate hypersensitive Th1- and Th2-type responses in subjects with asthma, which is likely an important mechanism in virus-induced asthma.

ACKNOWLEDGMENTS

REFERENCES

Adcock, I. M., Chung, K. F., Caramori, G., and Ito, K. (2006). Kinase inhibitors and airway inflammation. *Eur. J. Pharmacol.* 533, 118–132.

Azevedo, A. M., Durigon, E. L., Okasima, V., Queiroz, D. A., de Moraes-Vasconcelos, D., Duarte, A. J., and Grumach, A. S. (2003). Detection of influenza, parainfluenza, adenovirus and respiratory syncytial virus during asthma attacks in children older than 2 years old. *Allergol. Immunopathol. (Madr)* 31, 311–317.

Barnes, P. J. (2008). The cytokine network in asthma and chronic obstructive pulmonary disease. *J. Clin. Invest.* 118, 3546–3556.

Barrett, N. A., and Austen, K. F. (2009). Innate cells and T helper 2 cell immunity in airway inflammation. *Immunity* 31, 425–437.

Bousse, T., Chambers, R. L., Scroggs, R. A., Portner, A., and Takimoto, T. (2006). Human parainfluenza virus type 1 but not Sendai virus replicates in human respiratory cells despite IFN treatment. *Virus Res.* 121, 23–32.

Contoli, M., Message, S. D., Laza-Stanca, V., Edwards, M. R., Wark, P. A., Bartlett, N. W., Kebadze, T., Mallia, P., Stanciu, L. A., Parker, H. L., Slater, L., Lewis-Antes, A., Kon, O. M., Holgate, S. T., Davies, D. E., Kotenko, S. V., Papi, A., and Johnston, S. L. (2006). Role of deficient type III interferon-lambda production in asthma exacerbations. *Nat. Med.* 12, 1023–1026.

De, B. P., Galinski, M. S., and Banerjee, A. K. (1990). Characterization of an in vitro system for the synthesis of mRNA from human parainfluenza virus type 3. *J. Virol.* 64, 1135–1142.

de Oña, M., Melón, S., de la Iglesia, P., Hidalgo, F., and Verdugo, A. F. (1995). Isolation of influenza virus in human lung embryonated fibroblast cells (MRC-5) from clinical samples. *J. Clin. Microbiol.* 33, 1948–1949.

Folkerts, G., Busse, W. W., Nijkamp, F. P., Sorkness, R., and Gern, J. E. (1998). Virus-induced airway hyper-responsiveness and asthma. *Am. J. Respir. Crit. Care Med.* 157(Pt 1), 1708–1720.

Gehlhar, K., Bilitewski, C., Reinitz-Rademacher, K., Rohde, G., and Bufe, A. (2006). Impaired virus-induced interferon-alpha2 release in adult asthmatic patients. *Clin. Exp. Allergy* 36, 331–337.

Gern, J. E. (2009). Rhinovirus and the initiation of asthma. *Curr. Opin. Allergy Clin. Immunol.* 9, 73–78.

Hershenson, M. B., and Johnston, S. L. (2006). Rhinovirus infections: more than a common cold. *Am. J. Respir. Crit. Care Med.* 174, 1284–1285.

Hiscott, J., Kwon, H., and Génin, P. (2001). Hostile takeovers: viral appropriation of the NF-kappaB pathway. *J. Clin. Invest.* 107, 143–151.

Holgate, S. T. (2007). Epithelium dysfunction in asthma. *J. Allergy Clin. Immunol.* 120, 1233–1244.

Holgate, S. T., Davies, D. E., Rorke, S., Cakebread, J., Murphy, G., Powell, R. M., and Holloway, J. W. (2004a). ADAM 33 and its association with airway remodeling and hyperresponsiveness in asthma. *Clin. Rev. Allergy Immunol.* 27, 23–34.

Holgate, S. T., Holloway, J., Wilson, S., Bucchieri, F., Puddicombe, S., and Davies, D. E. (2004b). Epithelial–mesenchymal communication in the pathogenesis of chronic asthma. *Proc. Am. Thorac. Soc.* 1, 93–98.

Ishihara, C., Ochiai, K., Kagami, M., Takashahi, H., Matsuyama, G., Yoshida, S., Tomioka, H., and Koya, N. (1997). Human peripheral eosinophils express functional interferon-gamma receptors (IFN-gammaR). *Clin. Exp. Immunol.* 110, 524–529.

Ishioka, T., Kimura, H., Kita, H., Obuchi, M., Hoshino, H., Noda, M., Nishina, A., Kozawa, K., and Kato, M. (2010). Effects of respiratory syncytial virus infection and major basic protein derived from eosinophils in pulmonary alveolar epithelial cells (A549). *Cell Biol. Int.* (in press).

Jang, Y. J., Wang, J. H., Kim, J. S., Kwon, H. J., Yeo, N. K., and Lee, B. J. (2009). Levocetirizine inhibits rhinovirus-induced ICAM-1 and cytokine expression and viral replication in airway epithelial cells. *Antiviral Res.* 81, 226–233.

Johnston, S. L. (2004). Overview of virus-induced airway disease. *Proc. Am. Thorac. Soc.* 2, 150–156.

Khetsuriani, N., Kazerouni, N. N., Erdman, D. D., Lu, X., Redd, S. C., Anderson, L. J., and Teague, W. G. (2007). Prevalence of viral respiratory tract infections in children with asthma. *J. Allergy Clin. Immunol.* 119, 314–321.

Kohlmeier, J. E., Cookenham, T., Miller, S. C., Roberts, A. D., Christensen, J. P., Thomsen, A. R., and Woodland, D. L. (2009). CXCR3 directs antigen-specific effector CD4+ T cell migration to the lung during parainfluenza virus infection. *J. Immunol.* 183, 4378–4384.

Kotaniemi-Syrjänen, A., Vainionpää, R., Reijonen, T. M., Waris, M., Korhonen, K., and Korppi, M. (2003). Rhinovirus-induced wheezing in infancy--the first sign of childhood asthma? *J. Allergy Clin. Immunol.* 111, 66–71.

Krug, N., Madden, J., Redington, A. E., Lackie, P., Djukanovic, R., Schauer, U., Holgate, S. T., Frew, A. J., and

Howarth, P. H. (1996). T-cell cytokine profile evaluated at the single cell level in BAL and blood in allergic asthma. *Am. J. Respir. Cell Mol. Biol.* 14, 319–326.

Kusel, M. M., de Klerk, N. H., Kebadze, T., Vohma, V., Holt, P. G., Johnston, S. L., and Sly, P. D. (2007). Early-life respiratory viral infections, atopic sensitization, and risk of subsequent development of persistent asthma. *J. Allergy Clin. Immunol.* 119, 1105–1110.

Lee, D. C. W., and Lau, A. S. Y. (2007). Avian influenza virus signaling: implications for the disease severity of H5N1 infection. *Signal Transduct.* 7, 64–80.

Lemanske, R. F. Jr., Jackson, D. J., Gangnon, R. E., Evans, M. D., Li, Z., Shult, P. A., Kirk, C. J., Reisdorf, E., Roberg, K. A., Anderson, E. L., Carlson-Dakes, K. T., Adler, K. J., Gilbertson-White, S., Pappas, T. E., Dasilva, D. F., Tisler, C. J., and Gern, J. E. (2005). Rhinovirus illnesses during infancy predict subsequent childhood wheezing. *J. Allergy Clin. Immunol.* 116, 571–577.

MacMaster, J. F., Dambach, D. M., Lee, D. B., Berry, K. K., Qiu, Y., Zusi, F. C., and Burke, J. R. (2003). An inhibitor of IkappaB kinase, BMS-345541, blocks endothelial cell adhesion molecule expression and reduces the severity of dextran sulfate sodium-induced colitis in mice. *Inflamm. Res.* 52, 508–511.

Magnan, A. O., Mély, L. G., Camilla, C. A., Badier, M. M., Montero-Julian, F. A., Guillot, C. M., Casano, B. B., Prato, S. J., Fert, V., Bongrand, P., and Vervloet, D. (2000). Assessment of the Th1/Th2 paradigm in whole blood in atopy and asthma. Increased IFN-gamma-producing CD8(+) T cells in asthma. *Am. J. Respir. Crit. Care Med.* 161, 1790–1796.

Mallia, P., and Johnston, S. L. (2006). How viral infections cause exacerbation of airway diseases. *Chest* 130, 1203–1210.

Martinez, F. D. (2003). Respiratory syncytial virus bronchiolitis and the pathogenesis of childhood asthma. *Pediatr. Infect. Dis. J.* 22, S76–S82.

Matsuse, H., Kondo, Y., Saeki, S., Nakata, H., Fukushima, C., Mizuta, Y., and Kohno, S. (2005). Naturally occurring parainfluenza virus 3 infection in adults induces mild exacerbation of asthma associated with increased sputum concentrations of cysteinyl leukotrienes. *Int. Arch. Allergy Immunol.* 138, 267–272.

Message, S. D., and Johnston, S. L. (2004). Host defense function of the airway epithelium in health and disease: clinical background. *J. Leukoc. Biol.* 75, 5–17.

Monto, A. S. (2004). Occurrence of respiratory virus: time, place and person. *Pediatr. Infect. Dis. J.* 23(Suppl.), S58–S64.

Okazaki, K., Kondo, M., Kato, M., Kakinuma, R., Nishida, A., Noda, M., Taniguchi, K., and Kimura, H. (2008). Serum cytokine and chemokine profiles in neonates with meconium aspiration syndrome. *Pediatrics* 121, e748–e753.

Pelaia, G., Vatrella, A., Gallelli, L., Renda, T., Cazzola, M., Maselli, R., and Marsico, S. A. (2006). Respiratory infections and asthma. *Respir. Med.* 100, 775–784.

Proud, D., and Chow, C. W. (2006). Role of viral infections in asthma and chronic obstructive pulmonary disease. *Am. J. Respir. Cell Mol. Biol.* 35, 513–518.

Puxeddu, I., Bader, R., Piliponsky, A. M., Reich, R., Levi-Schaffer, F., and Berkman, N. (2006). The CC chemokine eotaxin/CCL11 has a selective profibrogenic effect on human lung fibroblasts. *J. Allergy Clin. Immunol.* 117, 103–110.

Santoro, M. G., Rossi, A., and Amici, C. (2003). NF-kappaB and virus infection: who controls whom. *EMBO J.* 22, 2552–2560.

Singh, A. M., Moore, P. E., Gern, J. E., Lemanske, R. F. Jr., and Hartert, T. V. (2007). Bronchiolitis to asthma: a review and call for studies of gene-virus interactions in asthma causation. *Am. J. Respir. Crit. Care Med.* 175, 108–119.

Stein, R. T., Sherrill, D., Morgan, W. J., Holberg, C. J., Halonen, M., Taussig, L. M., Wright, A. L., and Martinez, F. D. (1999). Respiratory syncytial virus in early life and risk of wheeze and allergy by age 13 years. *Lancet* 354, 541–545.

Stephan, L. (2007). Influenza viruses and MAP kinase cascades - Novel targets for an antiviral intervention? *Signal Transduct.* 7, 81–88.

Suzuki, K., Hino, M., Hato, F., Tatsumi, N., and Kitagawa, S. (1999). Cytokine-specific activation of distinct mitogen-activated protein kinase subtype cascades in human neutrophils stimulated by granulocyte colony-stimulating factor, granulocyte-macrophage colony-stimulating factor, and tumor necrosis factor-alpha. *Blood* 93, 341–349.

Thimmaiah, K. N., Easton, J. B., Germain, G. S., Morton, C. L., Kamath, S., Buolamwini, J. K., and Houghton, P. J. (2005). Identification of N10-substituted phenoxazines as potent and specific inhibitors of Akt signaling. *J. Biol. Chem.* 280, 31924–31935.

Ueba, O. (1978). Respiratory syncytial virus. I. Concentration and purification of the infectious virus. *Acta Med. Okayama* 32, 265–272.

Wark, P. A., Johnston, S. L., Bucchieri, F., Powell, R., Puddicombe, S., Laza-Stanca, V., Holgate, S. T., and Davies, D. E. (2005). Asthmatic bronchial epithelial cells have a deficient innate immune response to infection with rhinovirus. *J. Exp. Med.* 201, 937–947.

Watanabe, T., Yoshikawa, H., Abe, Y., Yamazaki, S., Uehara, Y., and Abe, T. (2003). Renal involvement in children with influenza A virus infection. *Pediatr. Nephrol.* 18, 541–544.

Wong, C. K., Wang, C. B., Ip, W. K., Tian, Y. P., and Lam, C. W. (2005). Role of p38 MAPK and NF-κB for chemokine release in coculture of human eosinophils and bronchial epithelial cells. *Clin. Exp. Immunol.* 139, 90–100.

Yoshizumi, M., Nakamura, T., Kato, M., Ishioka, T., Kozawa, K., Wakamatsu, K., and Kimura, H. (2008). Release of cytokines/chemokines and cell death in UVB-irradiated human keratinocytes, HaCaT. *Cell Biol. Int.* 32, 1405–1411.

Zaheer, R. S., Koetzler, R., Holden, N. S., Wiehler, S., and Proud, D. (2009). Selective transcriptional down-regulation of human rhinovirus-induced production of CXCL10 from airway epithelial cells via the MEK1 pathway. *J. Immunol.* 182, 4854–4864.

Laboratory and Epidemiology Communications

Phylogenetic Analysis of Human Metapneumovirus from Children with Acute Respiratory Infection in Yamaguchi, Japan, during Summer 2009

Shoichi Toda, Hirokazu Kimura[1], Masahiro Noda[2], Katsumi Mizuta[3], Tomomi Matsumoto, Eitaro Suzuki[4], and Komei Shirabe*

Division of Virology, Yamaguchi Prefectural Institute of Public Health and Environment, Yamaguchi 753-0821; [1]Infectious Disease Surveillance Center and [2]Department of Virology III, National Institute of Infectious Diseases, Tokyo 208-0011; [3]Yamagata Prefectural Institute of Public Health, Yamagata 990-0031; and [4]Suzuki Pediatric Clinic, Yamaguchi 755-0151, Japan

Communicated by Ichiro Kurane

(Accepted January 5, 2010)

Human metapneumovirus (hMPV) belongs to the family *Paramyxoviridae*, genus *Metapneumovirus*. It is an important causative agent of acute respiratory infections (ARIs) in humans (1) whose epidemiology in Japan is not known. To better understand the molecular epidemiology of domestic strains of hMPV, we performed phylogenetic analysis of hMPV detected from children with ARIs in Yamaguchi Prefecture during July and August 2009.

Table 1 shows patient and virus data. Virus RNA was extracted from throat swabs using a QIAamp Viral RNA Mini Kit (Qiagen, Germantown, Md., USA) and suspended in DNase/RNase-free water. After RNA extraction, reverse transcriptase-polymerase chain reaction (RT-PCR) was performed as previously described (2). Amplicons were purified using a MinElute PCR Purification Kit (Qiagen), and the nucleotide sequences were determined by direct sequencing (2). We performed phylogenetic analysis based on the F gene

of hMPV strains using Molecular Evolutionary Genetics Analysis (MEGA) software version 4 (3). Evolutionary distances were estimated using Kimura's two-parameter method, and a phylogenetic tree was constructed using the neighbor-joining method (4). The reliability of the tree was estimated using 1,000 bootstrap replications.

The phylogenetic tree revealed that 14 out of the 18 strains detected during the 2009 summer season were clustered in the A2 subgroup, 3 strains were in the B1 subgroup, and 1 strain was in the B2 subgroup (Fig. 1). The 14 strains clustered in subgroup A2 were further classified into 2 subclusters. The nucleotide identities among the strains within the subgroups were 98.4 to 100% for subgroup A2 and 100% for subgroup B1. The nucleotide identities among the strains within the two subclusters of the A2 subgroup were 99.7 and 100%, respectively. In one of the subclusters of the A2 subgroup to which 11 strains belonged, an epidemiological rela-

Table 1. Patient and human metapneumovirus data

Patient	Age (y)	Sex	Diagnosis	Onset date	Sampling date	Strain	Subgroup	GenBank accession no.
1	1	F	Bronchiolitis	28 Jul. 2009	29 Jul. 2009	Yamaguchi 09-01	A2	AB533235
2	1	F	Pneumonia	26 Jul. 2009	29 Jul. 2009	Yamaguchi 09-03	A2	AB533239
3	2	F	Pneumonia	27 Jul. 2009	29 Jul. 2009	Yamaguchi 09-04	A2	AB533236
4	5	F	Bronchiolitis	30 Jul. 2009	31 Jul. 2009	Yamaguchi 09-07	A2	AB533237
5	2	M	Bronchiolitis	31 Jul. 2009	1 Aug. 2009	Yamaguchi 09-09	A2	AB533238
6	3	M	Bronchiolitis	31 Jul. 2009	3 Aug. 2009	Yamaguchi 09-10	A2	AB533240
7	8	M	Pneumonia	4 Aug. 2009	6 Aug. 2009	Yamaguchi 09-13	A2	AB533241
8	4	M	Bronchiolitis	4 Aug. 2009	6 Aug. 2009	Yamaguchi 09-14	A2	AB533242
9	9	F	Bronchiolitis	2 Aug. 2009	3 Aug. 2009	Yamaguchi 09-15	B2	AB533243
10	2	F	Pneumonia	7 Aug. 2009	8 Aug. 2009	Yamaguchi 09-17	B1	AB533244
11	4	M	Pneumonia	9 Aug. 2009	10 Aug. 2009	Yamaguchi 09-20	A2	AB533245
12	3	F	Bronchiolitis	8 Aug. 2009	10 Aug. 2009	Yamaguchi 09-22	A2	AB533246
13	4	M	Bronchiolitis	8 Aug. 2009	11 Aug. 2009	Yamaguchi 09-26	A2	AB533247
14	1	F	Bronchiolitis	12 Aug. 2009	13 Aug. 2009	Yamaguchi 09-29	A2	AB533248
15	6	F	Pneumonia	11 Aug. 2009	13 Aug. 2009	Yamaguchi 09-30	B1	AB533249
16	3	M	Bronchiolitis	11 Aug. 2009	13 Aug. 2009	Yamaguchi 09-31	B1	AB533250
17	4	M	Pneumonia	19 Aug. 2009	21 Aug. 2009	Yamaguchi 09-37	A2	AB533251
18	0 (3 mo)	F	Bronchiolitis	19 Aug. 2009	21 Aug. 2009	Yamaguchi 09-38	A2	AB533252

*Corresponding author: Mailing address: Yamaguchi Prefectural Institute of Public Health and Environment, 2-5-67 Aoi, Yamaguchi-shi, Yamaguchi 753-0821, Japan. Tel: +81-83-922-7630, Fax: +81-83-922-7632, E-mail: shirabe.koumei@pref.yamaguchi.lg.jp
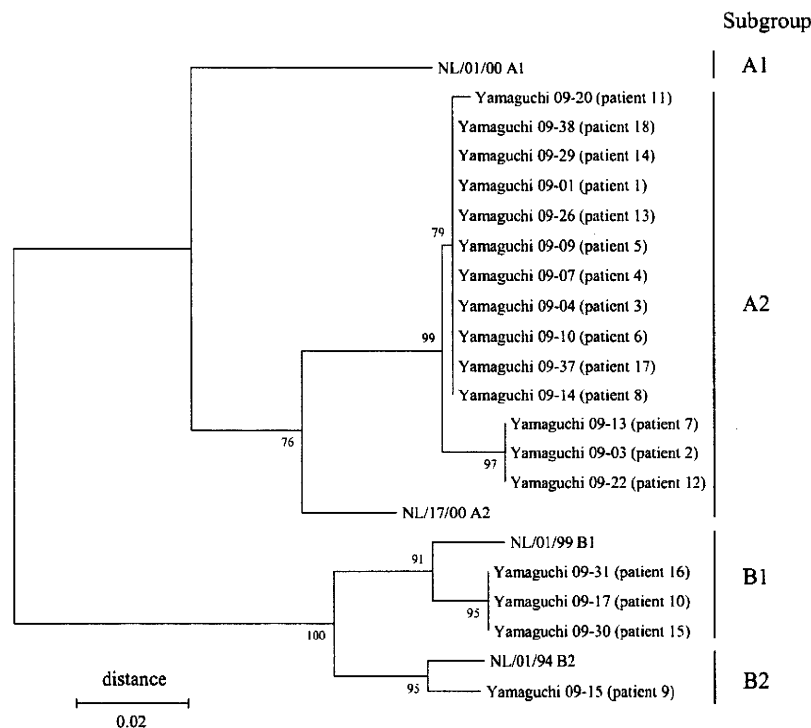
Fig. 1. Phylogenetic tree constructed on the basis of partial sequences of the human metapneumovirus F gene. Distance was calculated using Kimura's two-parameter method, and the tree was plotted using the neighbor-joining method. Numbers above the branches are bootstrap probabilities (%). Reference strains were NL/1/00, NL/17/00, NL/1/99, and NL/1/94.

tion was found. Five out of the 11 patients (patients 1, 4, 5, 6, and 13) and 2 patients (patients 8 and 14) attended the same nursery schools, respectively. In addition, patients 4 and 8 were from the same family. In the other subcluster, patients 2 and 12 attended the same nursery school, and patients 7 and 12 were from the same family.

In summary, hMPV was detected from a total of 18 children with ARIs during July and August 2009 in Yamaguchi Prefecture. All of these patients resided in the same city, indicating that a regional outbreak of hMPV occurred among the children. Phylogenetic analysis revealed that subgroup A2 was predominant in the outbreak, and that subgroups B1 and B2 cocirculated. Our findings suggested that this outbreak had at least four different infection sources. Although there have been few reports of hMPV being detected in the summer season (5-9), the results of the present study suggest that hMPV infections should be taken into consideration in children with ARIs throughout the year.

REFERENCES

1. Collins, P.L. and Crowe, J.E., Jr. (2007): Respiratory syncytial virus and metapneumovirus. p. 1601-1646. In D.M. Knipe and P.M. Howley (ed.), Fields Virology. vol. 1. 5th ed. Lippincott Williams & Wilkins, Philadelphia.
2. DiStefano, D.J., Kraiouchkine, N., Mallette, L., et al. (2005): Novel rotavirus VP7 typing assay using a one-step reverse transcriptase PCR protocol and product sequencing and utility of the assay for epidemiological studies and strain characterization, including serotype subgroup analysis. J. Clin. Microbiol., 43, 5876-5880.
3. Tamura, K., Dudley, J., Nei, M., et al. (2007): Molecular Evolutionary Genetics Analysis (MEGA) Software version 4.0. Mol. Biol. Evol., 24, 1596-1599.
4. Saitou, N. and Nei, M. (1987): The neighbor-joining method: a new method for reconstructing phylogenetic trees. Biol. Evol., 4, 406-425.
5. Abiko, C., Mizuta, K., Itagaki, T., et al. (2007): Outbreak of human metapneumovirus detected by use of the Vero E6 cell line in isolates collected in Yamagata, Japan, in 2004 and 2005. J. Clin. Microbiol., 45, 1912-1919.
6. Chano, F., Rousseau, C., Laferriére, C., et al. (2005): Epidemiological survey of human metapneumovirus infection in a large pediatric tertiary care center. J. Clin. Microbiol., 43, 5520-5525.
7. Osterhaus, A. and Fouchier, R. (2003): Human metapneumovirus in the community. Lancet, 361, 890-891.
8. van den Hoogen, B.G., van Doornum, G.J., Fockens, J.C., et al. (2003): Prevalence and clinical symptoms of human metapneumovirus infection in hospitalized patients. J. Infect. Dis., 188, 1571-1577.
9. Williams, J.V., Harris, P.A., Tollefson, S.J., et al. (2004): Human metapneumovirus and lower respiratory tract disease in otherwise healthy infants and children. N. Engl. J. Med., 350, 443-450.

Efficient Activation of the Severe Acute Respiratory Syndrome Coronavirus Spike Protein by the Transmembrane Protease TMPRSS2[▽]

Shutoku Matsuyama,[1]* Noriyo Nagata,[2] Kazuya Shirato,[1] Miyuki Kawase,[1] Makoto Takeda,[1] and Fumihiro Taguchi[3]

Departments of Virology III[1] and Pathology,[2] National Institute of Infectious Diseases, Japan, 4-7-1 Gakuen Musashi-Murayama, Tokyo 208-0011, Japan, and Faculty of Veterinary Medicine, Nippon Veterinary and Life Science University, 1-7-1 Sakai-minami Musasino, Tokyo 180-8602, Japan[3]

The distribution of the severe acute respiratory syndrome coronavirus (SARS-CoV) receptor, an angiotensin-converting enzyme 2 (ACE2), does not strictly correlate with SARS-CoV cell tropism in lungs; therefore, other cellular factors have been predicted to be required for activation of virus infection. In the present study, we identified transmembrane protease serine 2 (TMPRSS2), whose expression does correlate with SARS-CoV infection in the upper lobe of the lung. In Vero cells expressing TMPRSS2, large syncytia were induced by SARS-CoV infection. Further, the lysosome-tropic reagents failed to inhibit, whereas the heptad repeat peptide efficiently inhibited viral entry into cells, suggesting that TMPRSS2 affects the S protein at the cell surface and induces virus-plasma membrane fusion. On the other hand, production of virus in TMPRSS2-expressing cells did not result in S-protein cleavage or increased infectivity of the resulting virus. Thus, TMPRSS2 affects the entry of virus but not other phases of virus replication. We hypothesized that the spatial orientation of TMPRSS2 vis-a-vis S protein is a key mechanism underling this phenomenon. To test this, the TMPRSS2 and S proteins were expressed in cells labeled with fluorescent probes of different colors, and the cell-cell fusion between these cells was tested. Results indicate that TMPRSS2 needs to be expressed in the opposing (target) cell membrane to activate S protein rather than in the producer cell, as found for influenza A virus and metapneumoviruses. This is the first report of TMPRSS2 being required in the target cell for activation of a viral fusion protein but not for the S protein synthesized in and transported to the surface of cells. Our findings suggest that the TMPRSS2 expressed in lung tissues may be a determinant of viral tropism and pathogenicity at the initial site of SARS-CoV infection.

Angiotensin-converting enzyme 2 (ACE2) has been shown to be the functional receptor for severe acute respiratory syndrome coronavirus (SARS-CoV) (18, 24), the etiological agent of an acute infectious disease that spreads mainly via the respiratory route. Although ACE2 is present in the vascular endothelial cells of all organs, SARS-CoV is highly pathogenic only in the lungs (12). Furthermore, while ACE2 expression in the lung has been shown for both type I and type II pneumocytes (12), cell tropism of SARS-CoV does not strictly correlate with ACE2 expression, suggesting that other factors are required to explain the pathogenesis of this disease (8, 32). One such factor is the critical role played by host cellular proteases in the process of viral entry into cells. For example, a variety of proteases such as trypsin, tryptase Clara, miniplasmin, human airway trypsin-like protease (HAT), and TMPRSS2 (transmembrane protease, serine 2) are known to cleave the glycoprotein hemagglutinin (HA) of influenza A viruses, a prerequisite for the fusion between viral and host cell membranes and viral cell entry. Cleavage of HA is critical for viral infection, with the tissue distribution of proteases deter-

mining cell tropism of virus strains (16). There are two major mechanisms responsible for proteolytic activation of viral glycoproteins. For many viruses, such as the human immunodeficiency virus (HIV) and Nipah virus, cellular proteases (e.g., furin or cathepsin) cleave the glycoprotein during biogenesis, separating receptor binding and fusion subunits and converting the precursor glycoprotein to its fusion-competent state (36). Alternatively, for other viruses such as Ebola and SARS-CoV, cleavage of the viral glycoprotein by endosomal proteases induces conformational changes during viral entry following receptor binding and/or endocytosis (6, 20, 28, 31).

Three proteases—trypsin, cathepsin L, and elastase—have been previously reported to activate the spike (S) protein of SARS-CoV (3, 13, 20, 30, 31). In the absence of proteases at the cell surface, SARS-CoV enters cells by an endosomal pathway, and S protein is activated for fusion by cathepsin L in the endosome (14, 30, 37). Conversely, in the presence of proteases at the cell surface, such as trypsin and elastase, viral S proteins attached to the receptor at the host cell surface are activated, inducing envelope-plasma membrane fusion and direct entry of SARS-CoV into cells (21). Viral replication in the latter case has been shown to be 100 times higher than replication via the endosomal pathway (21), suggesting that the higher infectivity of SARS-CoV in the lungs could be due to an enhancement of direct viral cell entry mediated by proteases. In this study we test the possibility that TMPRSS2 is an acti-

* Corresponding author. Mailing address: Department of Virology III, National Institute of Infectious Diseases, Japan, 4-7-1 Gakuen, Musashi-Murayama, Tokyo 208-0011, Japan. Phone: 81 42 561 0771, ext. 3755. Fax: 81 42 567 5631. E-mail: matuyama@nih.go.jp.

vator of SARS-CoV entry into host cells. TMPRSS2 is highly expressed at epithelial cells in human lungs (9, 26) and activates influenza A virus and metapneumovirus in culture cells (4, 5, 7, 29). Here, we present data indicating that the distribution of TMPRSS2 correlates with SARS-CoV infection in the lung and that this protease can efficiently activate SARS-CoV S protein to induce virus-cell membrane fusion at the cell surface.

MATERIALS AND METHODS

Animal experiments. Animal experiments with SARS-CoV-infected cynomolgus monkeys were performed as described previously (23). Briefly, 3-year-old male cynomolgus monkeys were intratracheally inoculated with 108 50% tissue culture infective doses ($TCID_{50}$) of SARS-CoV. On day 7 postinoculation animals were euthanized, and tissue samples of the lungs were collected.

Immunofluorescence staining method. Detection of TMPRSS2, ACE2, and SARS-CoV antigens was performed on paraffin-embedded sections by a double immunofluorescence staining method modified from a previous protocol (19, 22, 23). Rabbit antibody (Ab) against TMPRSS2 (ab56110; Abcam), goat antibody against recombinant human ACE2 (R&D Systems, MN), and the SKOT9 monoclonal mouse antibody against nucleocapsid protein of SARS-CoV (25) were used as primary antibodies. Briefly, after deparaffinization with xylene, the sections were rehydrated in ethanol and immersed in phosphate-buffered saline (PBS). Antigens were retrieved by hydrolytic autoclaving in the retrieval solution at pH 9.0 (Nichirei). After a cooling step, normal donkey or goat serum was used to block background staining. To detect the TMPRSS2 or ACE2 antigen, the sections were immersed in PBS and then incubated with primary antibodies overnight at 4°C. After three washes in PBS, the sections were incubated with monoclonal antibody for 60 min at 37°C to detect the SARS-CoV protein. After three additional washes in PBS, the sections were incubated with anti-rabbit (goat origin) or anti-goat (donkey origin) Alexa Fluor 546 and anti-mouse (goat or donkey origin) Alexa Fluor 488 (Molecular Probes, Eugene, OR) for 60 min at 37°C to detect the primary antibodies,. The sections were mounted with ProLong antifade reagent with 4′,6′-diamidino-2-phenylindole (DAPI; Molecular Probes), and images were captured and analyzed by confocal laser microscopy (Fluoview FV1000-D; Olympus, Tokyo, Japan).

Cells and viruses. Vero E6 and Vero cells and Vero cells expressing TMPRSS2 (Vero-TMPRSS2) (29) were cultured in Dulbecco's modified Eagle's medium (DMEM; Gibco/BRL), supplemented with 5% fetal bovine serum (Gibco/BRL). The SARS-CoV Frankfurt 1 strain, kindly provided by J. Ziebuhr (University of Würzburg, Germany), and the recombinant vaccinia virus containing the gene encoding the spike protein of SARS-CoV (Dis/SARS-S), kindly provided by K. Ishii (NIID, Japan), were propagated and assayed by using Vero E6 and 293T cells, respectively.

Virus entry assay. Vero or Vero-TMPRSS2 cells in 96-well plates were treated with DMEM containing the reagents indicated in the legends of Fig. 3 at 37°C for 30 min and then chilled on ice for 10 min. Approximately 105 PFU (PFU) of virus in DMEM was used to infect 106 cells on ice. After an adsorption period of 30 min, the virus was removed, and infected cells were cultured in DMEM with the reagents at 37°C for 5 h. Viral mRNAs were isolated from cells with the addition of 200 μl of Isogen (Nippon gene). Real-time PCR was performed to estimate the amounts of newly synthesized mRNA9 as described previously (21).

Western blotting. Expression of S protein in Vero E6 cells was analyzed by Western blotting. Preparation of cell lysates, SDS-PAGE, and electrical transfer of the protein onto a transfer membrane were described elsewhere (21). S protein was detected with anti-S antibody (IMG-557; Imgenex, San Diego) and anti-rabbit IgG-horseradish peroxidase (HRPO). Influenza virus HA was detected with anti-HA Ab, Udorn virus HA (29), and anti-goat IgG-HRPO. Bands were visualized by using enhanced chemiluminescence reagents (ECL Plus; Amersham Pharmacia) on an LAS-1000 instrument (Fuji).

Cell-cell fusion. Effector cells (Vero or Vero-TMPRSS2) were infected with Dis/SARS-S at a multiplicity of infection (MOI) of 1 for 1 h or transfected with pKS/SARS-S by using the Fugene 6 reagent (Roche) and then labeled with 2 μM CellTracker Green (5-chloromethylfluorescein diacetate [CMFDA] Invitrogen) for 30 min and washed three times with medium. Meanwhile, Vero or Vero-TMPRSS2 target cells were labeled with 2 μM orange chloromethyl tetramethylrhodamine (CMTMR; Invitrogen) for 30 min and washed three times with medium. Effector cells were collected with nonenzymatic cell dissociation solution (Sigma) and then overlaid on target cells. Cells were incubated for 20 h and observed by fluorescence microscopy (BioZero, Keyence) for cell-cell fusion.

The extent of syncytium formation was semiquantified by counting the number of nuclei in the S-protein-expressing cells (10 syncytia).

RESULTS

Distribution of TMPRSS2 in the SARS-CoV-infected cynomolgus lung. We examined the immunohistochemical distribution of TMPRSS2 and ACE2 in the uninfected lung of cynomolgus monkeys. TMPRSS2 antigens were detected in type I pneumocytes (Fig. 1A, arrows indicating thin shapes in middle panel), whereas only weak staining of ACE2 antigens was detected in enlarged type II pneumocytes (Fig. 1C, arrows indicating round shapes in middle panel) by the immunofluorescence staining method used. An antibody against SARS-CoV was used as a negative control (Fig. 1A and C, upper left panels). In addition, the histopathology of SARS-CoV-infected lungs was examined on day 7 postinoculation as described previously (23). Mild lesions with some regenerated type II epithelial cells were observed in the upper lobe (Fig. 1B and D,). SARS-CoV antigens were detected in the cytoplasm of type I pneumocytes (Fig. 1B and D, arrowheads), which primarily resembled TMPRSS2-expressing cells (Fig. 1B, upper right) more than ACE2-expressing cells (Fig. 1D, upper right). In contrast, severe pulmonary edema and inflammatory reactions were observed in severe lesions (Fig. 1B and D). Marked immunostaining of TMPRSS2 and ACE2 antigens was detected in the cytoplasm of enlarged type II pneumocytes (Fig. 1B and D, lower middle panels). SARS-CoV antigens were detected in the cytoplasm of many unspecified cells (Fig. 1B and D, lower left), but these cells never merged with either TMPRSS2- or ACE2-expressing cells. These results suggest that the presence of SARS-CoV antigens does not correlate with the presence of either ACE2 or TMPRSS2 antigens in severe lesions.

Syncytium formation by SARS-CoV infection of TMPRSS2-expressing cells. Vero cells have been generally used for infection assays of SARS-CoV (10). SARS-CoV S protein-expressing Vero cells form syncytia if treated with trypsin but not in its absence (Fig. 2B, frames a and c). Here, we examined whether Vero cells stably expressing TMPRSS2 (VERO-TMPRSS2) undergo syncytium formation induced by SARS-CoV infection or S-protein expression. After 36 h of SARS-CoV infection at an MOI of 0.1, large syncytia were observed in Vero-TMPRSS2 cells (Fig. 2A, frame b) but not in Vero cells (Fig. 2A, frame a). To determine if expression of S protein induced syncytium formation, Vero-TMPRSS2 cells were infected with vaccinia virus encoding the SARS-CoV S gene, Dis/SARS-S, which resulted in the formation of large syncytia at 20 h after infection (Fig. 2B, frame b). In addition, plasmid-based expression of S protein also induced syncytia (see Fig. 5B). To further assess if TMPRSS2 can proteolytically activate S protein, Vero-TMPRSS2 cells expressing S protein were treated with various concentrations of leupeptin (Fig. 2C), a known inhibitor of serine and cysteine proteases. The results show that syncytium formation was moderately inhibited at a concentration of 500 μM (Fig. 2C, frame b, and D) and completely inhibited at a concentration of 5 mM (Fig. 2C, frame c, and D), suggesting that leupeptin inhibits the activity of TMPRSS2, suppressing S-protein-induced cell-cell fusion.
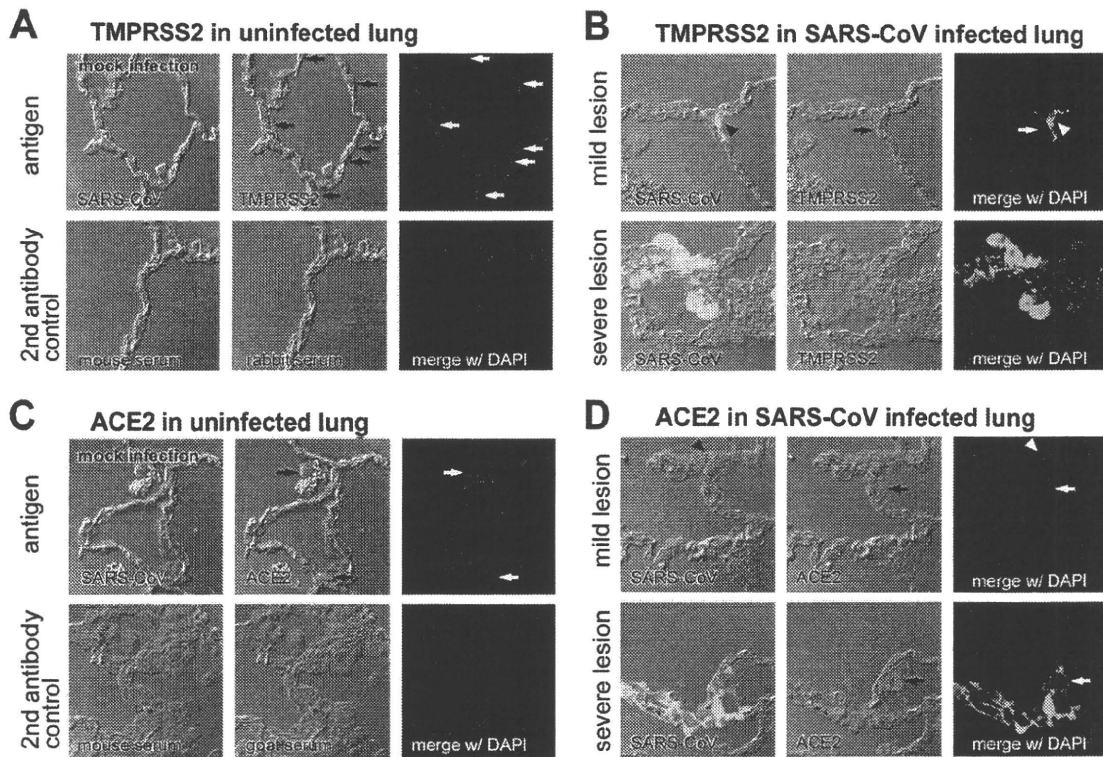
FIG. 1. Distribution of TMPRSS2 and ACE2 and histopathology of SARS-CoV-infected cynomolgus lung. The distribution of TMPRSS2 (A, arrows indicating round shapes in middle panel) and ACE2 (C, arrows indicating thin shapes in middle panel) in healthy cynomolgus lung sections stained with antibodies against SARS-CoV, TMPRSS2, or DAPI (upper panels) was detected by an immunofluorescence staining method (see Materials and Methods section). Samples stained with secondary antibodies were used as controls (lower panels). The distribution of TMPRSS2 (B) and ACE2 (D) was also examined in mild (upper row) and severe (lower row) lesions of SARS-CoV-infected lungs stained with antibodies against SARS-CoV, TMPRSS2, or DAPI (nuclear staining).

Viral entry into TMPRSS2-expressing cells. The above observations suggest that TMPRSS2 activates S protein at the cell surface, enabling viral entry into the cell. To assess this possibility, we first examined the effects of EST (Calbiochem), which is known to inhibit endosomal cathepsins and thereby block infection of Vero cells by SARS-CoV (35). Viral entry into cells was estimated by the newly synthesized viral mRNA9, which was quantified by real-time PCR as described previously (21). As shown in Fig. 3, treatment of Vero cells with EST at a concentration of 50 μM caused a 1,000-fold decrease of SARS-CoV cell entry via the endosomal pathway. In contrast, EST failed to suppress viral entry into Vero-TMPRSS2 cells. Similarly, treatment with bafilomycin A (Sigma) at a concentration of 500 μM reduced infectivity by 100-fold in Vero cells although only mild suppression (10%) of viral infection was observed in Vero-TMPRSS2 cells. Furthermore, we examined the effect of heptad repeat 2 (HR2) peptide, kindly provided by R. S. Hodges (33), on SARS-CoV infectivity in Vero-TMPRSS2 cells. HR2 peptide is known to prevent trypsin-activated cell entry of SARS-CoV via the cell surface; presumably an S protein activated by cell surface receptor exposes the HR1 region, and the HR2 peptide then interferes with the six-helix bundle formation (34). Treatment with HR2 peptide at a concentration of 5 μM efficiently suppressed viral entry into Vero-TMPRSS2 cells but not into Vero cells. These re-

sults suggest that TMPRSS2 activates S protein and facilitates viral entry via the cell surface.

TMPRSS2 does not cleave SARS-CoV S during virus production. It has been previously shown that TMPRSS2 expressed in cells promoted cleavage of glycoprotein of influenza A virus and metapneumovirus, increasing infectivity (5, 29). Here, we examined whether the S protein of SARS-CoV is cleaved and activated in Vero-TMPRSS2 cells. After 36 h of infection of Vero and Vero-TMPRSS2 cells with SARS-CoV, cells and medium were collected, and Western blotting was performed to detect S protein. As shown in Fig. 4A (right), the HA of influenza virus was markedly cleaved in Vero-TMPRSS2 cells at 18 h after transfection. However, S proteins synthesized in either Vero or Vero-TMPRSS2 cells were not cleaved when examined in cell lysates or in virions released into the medium (Fig. 4A, left). Furthermore, the infectious titers of SARS-CoV produced in Vero and Vero-TMPRSS2 (on Vero E6 cells) were not markedly different, and in both cases infection was inhibited by bafilomycin A1 but not HR2 peptide (Fig. 4B). These results suggest that SARS-CoV produced in Vero-TMPRSS2 cells has no fusion-competent, cleaved S protein entering into cells via the endosomal pathway.

Productive activation of S by TMPRSS2 requires TMPRSS2 expression in target cells. The previous results suggest that
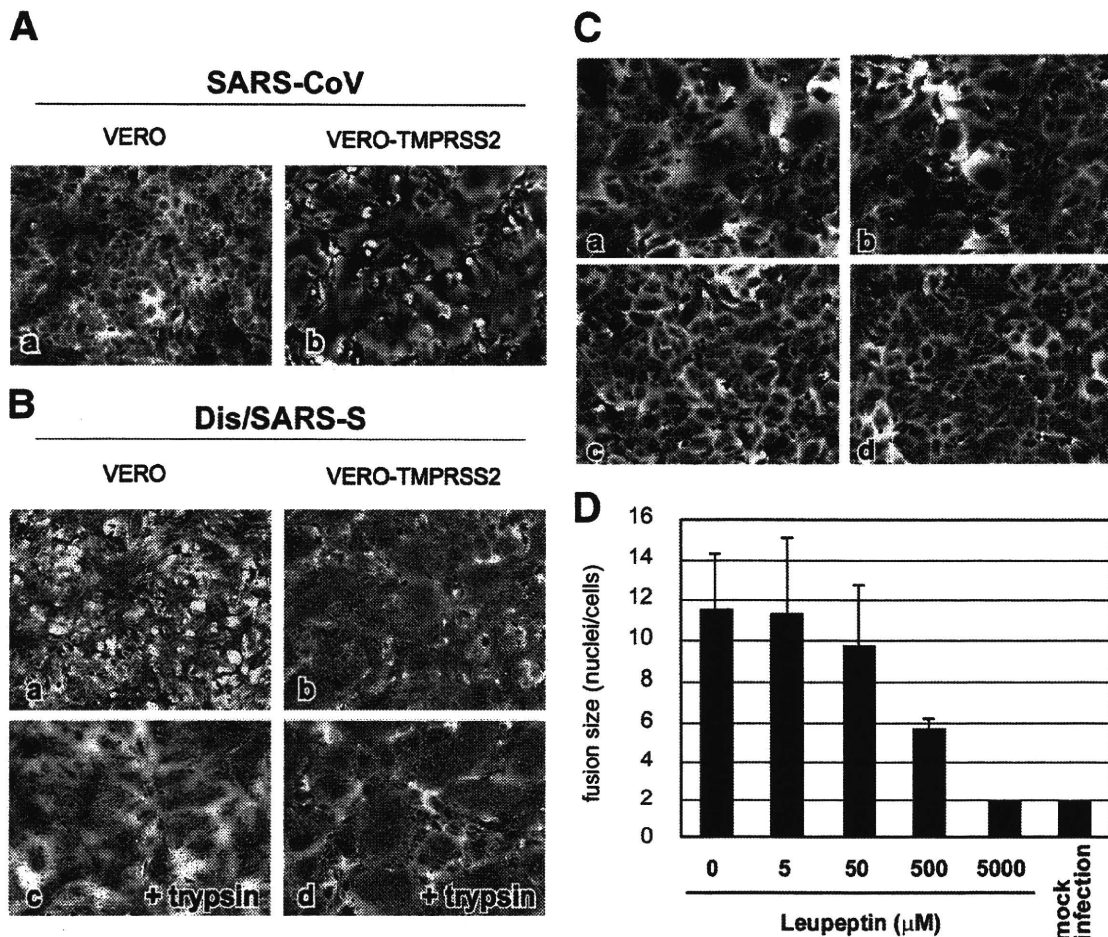
FIG. 2. Cytopathic changes on SARS-CoV S-protein-expressing cells. (A) Vero cells or Vero-TMPRSS2 cells were infected with SARS-CoV at an MOI of 0.1 and incubated at 37°C for 36 h. Cells were stained with crystal violet. (B) Vero cells or Vero-TMPRSS2 cells were infected with Dis/SARS-S at an MOI of 0.1 and incubated at 37°C for 20 h, after which the cells were treated with 10 μg/ml trypsin at 37°C for 30 min and then incubated for another 3 h. (C) Vero-TMPRSS2 cells were infected with Dis/SARS-S at an MOI of 0.1 and incubated at 37°C for 20 h in the absence (a) or presence of 500 μM (b) or 5 mM (c) leupeptin. Cells not infected with Dis/SARS-S were used as a control (d). (D) The size of syncytia in the absence and presence of 5 μM, 50 μM, 500 μM, and 5 mM leupeptin was quantified by counting the number of nuclei in the fused cells. The error bars are standard deviations.
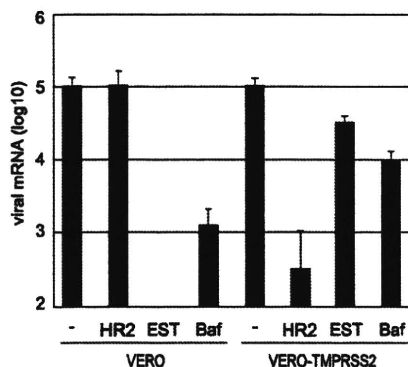

FIG. 3. Effect of TMPRSS2 on virus entry into cells. Vero or Vero-TMPRSS2 cells were infected with SARS-CoV at an MOI of 0.1 in the presence of 5 μM HR2 peptide, 50 μM EST, or 500 μM bafilomycin A1 and then cultured for 5 h. The amount of viral mRNA9 was measured by real-time PCR. Cells not treated with reagents were used as controls. The error bars are standard deviations of at least six independent measurements.

TMPRSS2 affects viral S protein attached to receptors at the cell surface but not newly synthesized S proteins either during transport to the plasma membrane or incorporation into the virion. We hypothesized that the spatial orientation of TMPRSS2 against S protein might be critical for S protein activation. To demonstrate this spatial dependence between TMPRSS2 and S protein, a cell-cell fusion assay was conducted. Our design is diagramed in Fig. 5A. Vero and Vero-TMPRSS2 cells were either Dis/SARS-S infected (Fig. 5B, frames a, b, c, and d) or pKS/SARS-S transfected (Fig. 5B, frames e, f, g, and h) to express S protein and then stained with green as described in the methodology. The green-labeled Vero and Vero-TMPRSS2 cells were collected with nonenzymatic cell dissociation solution and overlaid onto the orange-labeled target cells, Vero and Vero-TMPRSS2. As shown in Fig. 5B, the formation of syncytia was not induced in cells not expressing TMPRSS2 (Fig. 5B, frames a and e). Also, syncytia were not formed between green cells expressing
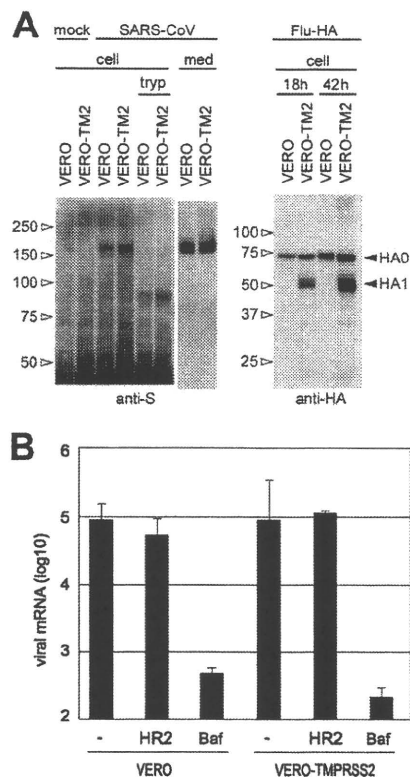
FIG. 4. TMPRSS2 does not affect virus production. (A) SDS-PAGE and Western blot analysis were performed to detect S protein in cell lysates (cell) and culture medium (med) of Vero or Vero-TMPRSS2 (Vero-TM2) cells at 20 h after SARS-CoV infection (left panel). Cells treated with 10 μg/ml trypsin (tryp) at 37°C for 5 min were used as a cleaved-S control. Influenza virus (Flu)-HA produced by plasmid transfection was also used as a cleavage control (right panel). (B) Infectivity of SARS-CoV produced in Vero or Vero-TMPRSS2 cells. Vero-E6 cells were infected with SARS-CoV produced in either Vero or Vero-TMPRSS2 cells in the presence of 5 μM HR2 peptide or 500 nM bafilomycin A1 and then cultured for 5 h. The amount of viral mRNA9 was measured by real-time PCR. Cells not treated with reagents were used as controls. The error bars are standard deviations of at least six independent measurements.

both TMPRSS2 and S protein and the orange Vero cells without TMPRSS2 (Fig. 5B, frames b and f). However, large syncytia were formed when TMPRSS2 was expressed either in the orange target cells (Fig. 5B, frames c and g) or both in the orange target and green producer cells (Fig. 5B, frames d and h). The extent of syncytium formation was semiquantified by counting the number of nuclei in the fused cells infected with Dis/SARS-S (Fig. 5C). It was previously reported that ACE2 is downregulated in S-expressing cells (11, 17), indicating that green producer cells are refractory to self-fusion due to a lack of receptors at the cell surface. These results suggest that the spatial orientation of TMPRSS2 must be opposite that of S protein (namely, the two proteins must reside in opposite membranes) to induce membrane fusion. This observation is in agreement with the idea that TMPRSS2 activates only viral S protein already attached to receptors at the cell surface but not during virus maturation.
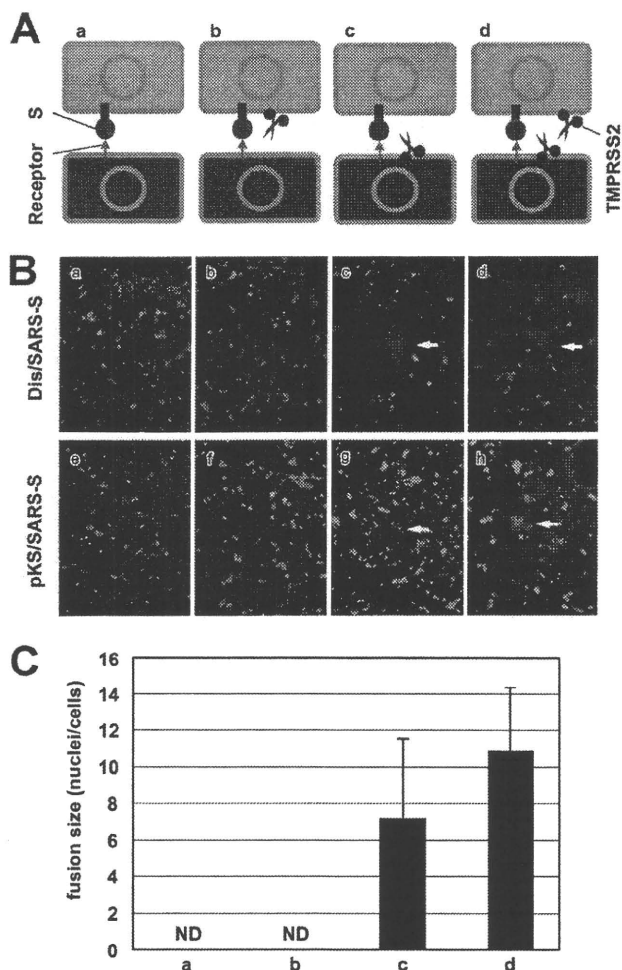
FIG. 5. TMPRSS2 dependence on spatial orientation for the activation of SARS-CoV S protein. (A) Schematic diagrams of S-expressing effector cells (green) and acceptor cells (orange) shown in panel B. (B) To detect cell-cell fusion of S-expressing cells, Dis/SARS-S-infected or pKS/SARS-S-transfected Vero or Vero-TMPRSS2 cells (effector cells) were collected by nonenzymatic cell dissociation solution and then overlaid onto the orange target Vero or Vero-TMPRSS2 cells, respectively. After 20 h of incubation, cells were fixed with 4% formaldehyde and observed by fluorescence microscopy. White arrows indicate fused cells. (C) The sizes of syncytia indicated in the upper row of panel B were quantified by counting the number of nuclei in the fused cells. The error bars are standard deviations.

DISCUSSION

In the present study we showed the distribution of ACE2 in mild and severe inflammatory lesions of cynomolgus lungs infected by SARS-CoV. We found that type II pneumocytes, which are frequently observed in regenerated tissues during inflammation and which express high levels of ACE2, were refractory to SARS-CoV infection, whereas type I pneumocytes, which do not express detectable levels of ACE2, were readily infected by SARS-CoV. This inconsistency may be explained by the downregulation of ACE2 in SARS-CoV-infected cells, as previously reported (11, 17). Here, we showed that the localization of TMPRSS2-expressing cells in normal lung tissues, rather than ACE2-expressing cells, is closely tied

to SARS-CoV infection in mild lesions, indicating that TM-PRSS2 may determine viral tropism at an early stage of SARS-CoV infection. However, TMPRSS2 expression occurred in cells adjacent to virus-infected cells, not in infected cells, suggesting that TMPRSS2 may also be downregulated in infected cells, as observed for ACE2. We have previously reported that SARS-CoV infectivity was enhanced in culture cells by the addition of exogenous elastase, which enabled virus entry via the cell surface (21). Elastase is a major protease produced by neutrophils during inflammation and may be relevant to the high level of SARS-CoV replication in lungs that results in severe pneumonia in the mouse model (1). We have also reported that in the late stage of SARS-CoV infection in the cynomolgus lung, which remarkably occurs with severe inflammation in the lower lobe, SARS-CoV is distributed in both type I and type II pneumocytes (23), indicating that elastase may trigger viral entry via the surface of these cells and determine SARS-CoV pathogenicity in this late stage of infection.

Activation of viral glycoprotein by TMPRSS2 has been previously reported for influenza A virus and metapneumovirus (4, 5, 7, 29). The most distinctive difference between these viruses and SARS-CoV is the stage during virus replication in which viral glycoproteins are cleaved by proteases. In influenza A virus and metapneumovirus, the protease makes a simple cut in the glycoprotein during maturation, in a manner similar to that made by furin. In contrast, SARS-CoV S protein is cleaved by the protease following receptor-induced conformational changes. The protease cleavage site in S protein, located nearer the C-terminal region than predicted for a cleavage site, is thought to be exposed only after receptor binding (2, 35). In support of this model, we recently reported that the S protein of mouse hepatitis virus type 2 (MHV-2), which is highly similar to the S protein of SARS-CoV (27), requires two-step conformational changes mediated by sequential receptor binding and proteolysis to be activated for fusion (20). Such a mechanism allows for tight temporal control over fusion by protecting the activating cleavage site from premature proteolysis yet allowing efficient cleavage upon binding to the receptor on target cells.

Previous studies have clearly demonstrated that the SARS-CoV S protein requires proteolytic cleavage for S-mediated cell-cell or virus-cell fusion (3, 13, 21, 30, 31). Recently, the cleavage of S protein by the airway transmembrane protease, TMPRSS11a, was also reported (15). Treatment with a purified soluble form of TMPRSS11a following receptor binding to the pseudotyped SARS-CoV S protein strongly enhanced viral infection. Moreover, proteolytic cleavage by TMPRSS11a was observed at the same position as cleavage by trypsin in the purified soluble form of S protein (15). While the reported concentration of the previously mentioned proteases required to induce membrane fusion is extremely high (3, 15, 21), the amount of TMPRSS2 expressed in Vero-TMPRSS2 cells is thought to be low (29). Still, our results showed the formation of massive syncytia when S protein was expressed (Fig. 2), suggesting that TMPRSS2 may be more efficient than previously characterized proteases. The inhibition of cell-cell fusion in TMPRSS2-expressing cells in the presence of a protease inhibitor (Fig. 2) strongly suggests that TMPRSS2 proteolytically affects S protein. Because we could not detect a consid-

erable amount of cleaved S protein in cells expressing both S and TMPRSS2, even when massive syncytia were observed in these cells, we hypothesized that proteolytic activation of S protein by TMPRSS2 occurs only during cell entry, following receptor binding. The results shown in Fig. 5 support this hypothesis and clearly show that the spatial orientation of TMPRSS2 in relation to S protein is a key mechanism underling this phenomenon: TMPRSS2 must be expressed in the opposing cell membrane to activate S protein and induce cell-cell fusion. We speculate that the encounter of receptor-bound S protein with TMPRSS2 at the right time and in the correct spatial orientation at the cell surface results in efficient cleavage of S protein and subsequent membrane fusion. Therefore, only a small amount of S protein needs to be cleaved to enable viral or cell-cell membrane fusion. These cleavage products would be difficult to detect by Western blot analysis.

Additionally, we have previously reported that HR2 peptide inhibits SARS-CoV entry into Vero E6 cells in the presence, but not the absence, of trypsin. Likewise, inhibition of SARS-CoV cell entry does not occur when the virus is allowed to use the normal endosomal, cathepsin L-dependent, entry pathway (34). Here, we show (Fig. 3) that HR2 peptide efficiently inhibits viral entry into TMPRSS2-expressing cells. This result provides further evidence that TMPRSS2 is efficient for viral entry and is localized at the cell surface, exposing the HR2 peptide binding site before endocytosis can occur. Thus, even if HR2 peptide does not efficiently work in commonly used tissue cell cultures, it may be a suitable candidate antiviral for the inhibition of SARS-CoV infection of lung cells that express membrane-associated proteases.

REFERENCES

1. **Ami, Y., N. Nagata, K. Shirato, R. Watanabe, N. Iwata, K. Nakagaki, S. Fukushi, M. Saijo, S. Morikawa, and F. Taguchi.** 2008. Co-infection of respiratory bacterium with severe acute respiratory syndrome coronavirus induces an exacerbated pneumonia in mice. Microbiol. Immunol. 52:118–127.

2. **Belouzard, S., V. C. Chu, and G. R. Whittaker.** 2009. Activation of the SARS coronavirus spike protein via sequential proteolytic cleavage at two distinct sites. Proc. Natl. Acad. Sci. U. S. A. 106:5871–5876.

3. **Bosch, B. J., W. Bartelink, and P. J. M. Rottier.** 2008. Cathepsin L functionally cleaves the severe acute respiratory syndrome coronavirus class I fusion protein upstream of rather than adjacent to the fusion peptide. J. Virol. 82:8887–8890.

4. **Böttcher, E., T. Matrosovich, M. Beyerle, H. Klenk, W. Garten, and M. Matrosovich.** 2006. Proteolytic activation of influenza viruses by serine proteases TMPRSS2 and HAT from human airway epithelium. J. Virol. 80:9896–9898.

5. **Chaipan, C., D. Kobasa, S. Bertram, I. Glowacka, I. Steffen, T. S. Tsegaye, M. Takeda, T. H. Bugge, S. Kim, Y. Park, A. Marzi, and S. Pöhlmann.** 2009. Proteolytic activation of the 1918 influenza virus hemagglutinin. J. Virol. 83:3200–3211.

6. **Chandran, K., N. J. Sullivan, U. Felbor, S. P. Whelan, and J. M. Cunningham.** 2005. Endosomal proteolysis of the Ebola virus glycoprotein is necessary for infection. Science 308:1643–1645.

7. **Choi, S., S. Bertram, I. Glowacka, Y. W. Park, and S. Pöhlmann.** 2009. Type II transmembrane serine proteases in cancer and viral infections. Trends Mol. Med. 15:303–312.

8. **Ding, Y., H. Wang, H. Shen, Z. Li, J. Geng, H. Han, J. Cai, X. Li, W. Kang,**

D. Weng, Y. Lu, D. Wu, L. He, and K. Yao. 2003. The clinical pathology of severe acute respiratory syndrome (SARS): a report from China. J. Pathol. 200:282–289.

9. Donaldson, S. H., A. Hirsh, D. C. Li, G. Holloway, J. Chao, R. C. Boucher, and S. E. Gabriel. 2002. Regulation of the epithelial sodium channel by serine proteases in human airways. J. Biol. Chem. 277:8338–8345.

10. Drosten, C., S. Günther, W. Preiser, S. van der Werf, H. R. Brodt, S. Becker, H. Rabenau, M. Panning, L. Kolesnikova, R. A. Fouchier, A. Berger, A. M. Burguière, J. Cinatl, M. Eickmann, N. Escriou, K. Grywna, S. Kramme, J. C. Manuguerra, S. Müller, V. Rickerts, M. Stürmer, S. Vieth, H. D. Klenk, A. D. Osterhaus, H. Schmitz, and H. W. Doerr. 2003. Identification of a novel coronavirus in patients with severe acute respiratory syndrome. N. Engl. J. Med. 348:1967–1976.

11. Glowacka, I., S. Bertram, P. Herzog, S. Pfefferle, I. Steffen, M. O. Muench, G. Simmons, H. Hofmann, T. Kuri, F. Weber, J. Eichler, C. Drosten, and S. Pöhlmann. 2010. Differential downregulation of ACE2 by the spike proteins of SARS-coronavirus and human coronavirus NL63. J. Virol. 84:1198–1205.

12. Hamming, I., W. Timens, M. L. C. Bulthuis, A. T. Lely, G. J. Navis, and H. van Goor. 2004. Tissue distribution of ACE2 protein, the functional receptor for SARS coronavirus. A first step in understanding SARS pathogenesis. J. Pathol. 203:631–637.

13. Huang, I., B. J. Bosch, F. Li, W. Li, K. H. Lee, S. Ghiran, N. Vasilieva, T. S. Dermody, S. C. Harrison, P. R. Dormitzer, M. Farzan, P. J. M. Rottier, and H. Choe. 2006. SARS coronavirus, but not human coronavirus NL63, utilizes cathepsin L to infect ACE2-expressing cells. J. Biol. Chem. 281:3198–3203.

14. Inoue, Y., N. Tanaka, Y. Tanaka, S. Inoue, K. Morita, Z. Min, T. Hattori, and K. Sugamura. 2007. Clathrin-dependent entry of severe acute respiratory syndrome coronavirus into target cells expressing ACE2 with the cytoplasmic tail deleted. J. Virol. 81:8722–8729.

15. Kam, Y., Y. Okumura, H. Kido, L. F. P. Ng, R. Bruzzone, and R. Altmeyer. 2009. Cleavage of the SARS coronavirus spike glycoprotein by airway proteases enhances virus entry into human bronchial epithelial cells in vitro. PloS One 4:e7870.

16. Kido, H., Y. Okumura, E. Takahashi, H. Pan, S. Wang, J. Chida, T. Q. Le, and M. Yano. 2008. Host envelope glycoprotein processing proteases are indispensable for entry into human cells by seasonal and highly pathogenic avian influenza viruses. J. Mol. Gen. Med. 3:167–175.

17. Kuba, K., Y. Imai, S. Rao, H. Gao, F. Guo, B. Guan, Y. Huan, P. Yang, Y. Zhang, W. Deng, L. Bao, B. Zhang, G. Liu, Z. Wang, M. Chappell, Y. Liu, D. Zheng, A. Leibbrandt, T. Wada, A. Slutsky, D. Liu, C. Qin, C. Jiang, and J. Penninger. 2005. A crucial role of angiotensin converting enzyme 2 (ACE2) in SARS coronavirus-induced lung injury. Nat. Med. 11:875–879.

18. Li, W., M. Moore, N. Vasilieva, J. Sui, S. K. Wong, M. Berne, M. Somasundaran, J. Sullivan, K. Luzuriaga, T. Greenough, H. Choe, and M. Farzan. 2003. Angiotensin-converting enzyme 2 is a functional receptor for the SARS coronavirus. Nature 426:450–454.

19. Liem, N. T., N. Nakajima, L. P. Phat, Y. Sato, H. N. Thach, P. V. Hung, L. T. San, H. Katano, T. Kumasaka, T. Oka, S. Kawachi, T. Matsushita, T. Sata, K. Kudo, and K. Suzuki. 2008. H5N1-infected cells in lung with diffuse alveolar damage in exudative phase from a fatal case in Vietnam. Jpn. J. Infect. Dis. 61:157–160.

20. Matsuyama, S., and F. Taguchi. 2009. Two-step conformational changes in a coronavirus envelope glycoprotein mediated by receptor binding and proteolysis. J. Virol. 83:11133–11141.

21. Matsuyama, S., M. Ujike, S. Morikawa, M. Tashiro, and F. Taguchi. 2005. Protease-mediated enhancement of severe acute respiratory syndrome coronavirus infection. Proc. Natl. Acad. Sci. U. S. A. 102:12543–12547.

22. Nagata, N., N. Iwata, H. Hasegawa, S. Fukushi, A. Harashima, Y. Sato, M. Saijo, F. Taguchi, S. Morikawa, and T. Sata. 2008. Mouse-passaged severe acute respiratory syndrome-associated coronavirus leads to lethal pulmonary edema and diffuse alveolar damage in adult but not young mice. Am. J. Pathol. 172:1625–1637.

23. Nagata, N., N. Iwata, H. Hasegawa, Y. Sato, S. Morikawa, M. Saijo, S.

Itamura, T. Saito, Y. Ami, T. Odagiri, M. Tashiro, and T. Sata. 2007. Pathology and virus dispersion in cynomolgus monkeys experimentally infected with severe acute respiratory syndrome coronavirus via different inoculation routes. Int. J. Exp. Pathol. 88:403–414.

24. Nie, Y., P. Wang, X. Shi, G. Wang, J. Chen, A. Zheng, W. Wang, Z. Wang, X. Qu, M. Luo, L. Tan, X. Song, X. Yin, J. Chen, M. Ding, and H. Deng. 2004. Highly infectious SARS-CoV pseudotyped virus reveals the cell tropism and its correlation with receptor expression. Biochem. Biophys. Res. Commun. 321:994–1000.

25. Ohnishi, K., M. Sakaguchi, T. Kaji, K. Akagawa, T. Taniyama, M. Kasai, Y. Tsunetsugu-Yokota, M. Oshima, K. Yamamoto, N. Takasuka, S. Hashimoto, M. Ato, H. Fujii, Y. Takahashi, S. Morikawa, K. Ishii, T. Sata, H. Takagi, S. Itamura, T. Odagiri, T. Miyamura, I. Kurane, M. Tashiro, T. Kurata, H. Yoshikura, and T. Takemori. 2005. Immunological detection of severe acute respiratory syndrome coronavirus by monoclonal antibodies. Jpn. J. Infect. Dis. 58:88–94.

26. Paoloni-Giacobino, A., H. Chen, M. C. Peitsch, C. Rossier, and S. E. Antonarakis. 1997. Cloning of the TMPRSS2 gene, which encodes a novel serine protease with transmembrane, LDLRA, and SRCR domains and maps to 21q22.3. Genomics 44:309–320.

27. Qiu, Z., S. T. Hingley, G. Simmons, C. Yu, J. Das Sarma, P. Bates, and S. R. Weiss. 2006. Endosomal proteolysis by cathepsins is necessary for murine coronavirus mouse hepatitis virus type 2 spike-mediated entry. J. Virol. 80:5768–5776.

28. Schornberg, K., S. Matsuyama, K. Kabsch, S. Delos, A. Bouton, and J. White. 2006. Role of endosomal cathepsins in entry mediated by the Ebola virus glycoprotein. J. Virol. 80:4174–4178.

29. Shirogane, Y., M. Takeda, M. Iwasaki, N. Ishiguro, H. Takeuchi, Y. Nakatsu, M. Tahara, H. Kikuta, and Y. Yanagi. 2008. Efficient multiplication of human metapneumovirus in Vero cells expressing the transmembrane serine protease TMPRSS2. J. Virol. 82:8942–8946.

30. Simmons, G., D. N. Gosalia, A. J. Rennekamp, J. D. Reeves, S. L. Diamond, and P. Bates. 2005. Inhibitors of cathepsin L prevent severe acute respiratory syndrome coronavirus entry. Proc. Natl. Acad. Sci. U. S. A. 102:11876–11881.

31. Simmons, G., J. D. Reeves, A. J. Rennekamp, S. M. Amberg, A. J. Piefer, and P. Bates. 2004. Characterization of severe acute respiratory syndrome-associated coronavirus (SARS-CoV) spike glycoprotein-mediated viral entry. Proc. Natl. Acad. Sci. U. S. A. 101:4240–4245.

32. To, K. F., and A. W. I. Lo. 2004. Exploring the pathogenesis of severe acute respiratory syndrome (SARS): the tissue distribution of the coronavirus (SARS-CoV) and its putative receptor, angiotensin-converting enzyme 2 (ACE2). J. Pathol. 203:740–743.

33. Tripet, B., D. J. Kao, S. A. Jeffers, K. V. Holmes, and R. S. Hodges. 2006. Template-based coiled-coil antigens elicit neutralizing antibodies to the SARS-coronavirus. J. Struct. Biol. 155:176–194.

34. Ujike, M., H. Nishikawa, A. Otaka, N. Yamamoto, N. Yamamoto, M. Matsuoka, E. Kodama, N. Fujii, and F. Taguchi. 2008. Heptad repeat-derived peptides block protease-mediated direct entry from the cell surface of severe acute respiratory syndrome coronavirus but not entry via the endosomal pathway. J. Virol. 82:588–592.

35. Watanabe, R., S. Matsuyama, K. Shirato, M. Maejima, S. Fukushi, S. Morikawa, and F. Taguchi. 2008. Entry from the cell surface of severe acute respiratory syndrome coronavirus with cleaved S protein as revealed by pseudotype virus bearing cleaved S protein. J. Virol. 82:11985–11991.

36. White, J., S. Delos, M. Brecher, and K. Schornberg. 2008. Structures and mechanisms of viral membrane fusion proteins: multiple variations on a common theme. Crit. Rev. Biochem. Mol. Biol. 43:189–219.

37. Yang, Z., Y. Huang, L. Ganesh, K. Leung, W. Kong, O. Schwartz, K. Subbarao, and G. J. Nabel. 2004. pH-dependent entry of severe acute respiratory syndrome coronavirus is mediated by the spike glycoprotein and enhanced by dendritic cell transfer through DC-SIGN. J. Virol. 78:5642–5650.

JOURNAL OF MEDICAL
CASE REPORTS

CASE REPORT   **Open Access**

Endoscopic therapy using an endoscopic variceal ligation for minute cancer of the esophagogastric junction complicated with esophageal varices: a case report

Tomoyuki Akiyama[1], Yasunobu Abe[1], Hiroshi Iida[1], Hiroki Endo[1], Kunihiro Hosono[1], Kyoko Yoneda[1], Hirokazu Takahashi[1], Masahiko Inamori*[1], Akihide Ryo[2], Shoji Yamanaka[2], Yoshiaki Inayama[2] and Atsushi Nakajima[1]

Abstract

Introduction: Standard endoscopic mucosal resection or endoscopic submucosal dissection is a procedure for patients with minute cancers, complicated with esophageal varices that puts them at high risk of bleeding.

Case presentation: We present the case of a 77-year-old Japanese man with alcoholic cirrhosis who underwent a routine endoscopy examination as a screening procedure for esophageal varices and was incidentally diagnosed as having minute cancer of the esophagogastric junction with esophageal varices. Endoscopic ultrasonography findings suggested that the minute cancer was a non-invasive carcinoma (carcinoma in situ) and a 2 mm in diameter blood vessel, feeding the esophageal varices, pierced the lesion. Following the examination, we carried out endoscopic treatment of the minute cancer and esophageal varices. Endoscopic variceal ligation was performed using a pneumo-activated device (Sumitomo Bakelite, Tokyo, Japan). Two years after the treatment, during the follow-up endoscopic examination on the patient, recurrence of carcinoma was not detected endoscopically or histologically.

Conclusion: Endoscopic therapy using an endoscopic variceal ligation device for minute cancer of the esophagogastric junction, complicated with esophageal varices, may be an acceptable and easily applicable method.

Introduction

Minute cancer is a gastric cancer lesion of less than 5 mm in its maximum diameter, with tumor cells confined to the mucosa. Lymph node metastases, meanwhile, are extremely rare [1,2]. These characteristics of minute cancer provide the basis for using endoscopic therapy as a curative treatment [3]. In this report, we describe endoscopic therapy using an endoscopic variceal ligation (EVL) device for minute cancer complicated with esophageal varices.

Case presentation

A 77-year-old Japanese man with alcoholic cirrhosis had been undergoing a follow-up laboratory examination every month for three years. He had been undergoing

* Correspondence: inamorim@med.yokohama-cu.ac.jp
[1] Gastroenterology Division, Yokohama City University School of Medicine, Japan
Full list of author information is available at the end of the article

imaging studies such as ultrasonography and computed tomography every month as screening procedures for hepatocellular carcinoma, and endoscopic examination every year to monitor esophageal varices. During one such routine examination, he was diagnosed as having minute cancer of the esophagogastric junction (EGJ) (Figure 1) based on the histological examination of the biopsy specimen (Figure 2) and esophageal varices (Figure 3). One month later, he was referred to our institution for endoscopic ultrasonography (EUS) evaluation (Olympus UM2000, Olympus Optical Company, Tokyo, Japan) and endoscopic therapy. The ultrasonography findings showed that the minute cancer was a noninvasive carcinoma (carcinoma in situ) and a blood vessel, 2 mm in diameter feeding the esophageal varices, pierced the lesion (Figure 4).
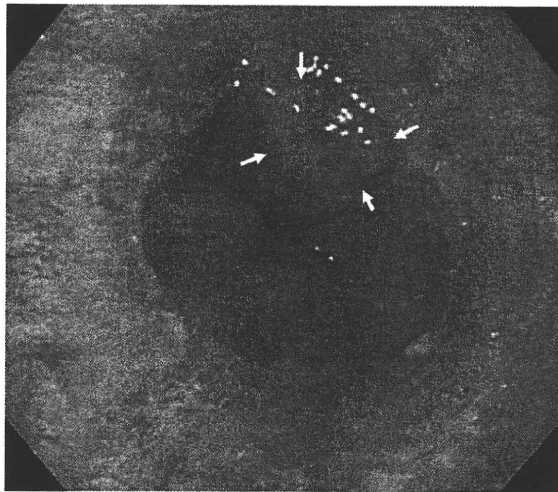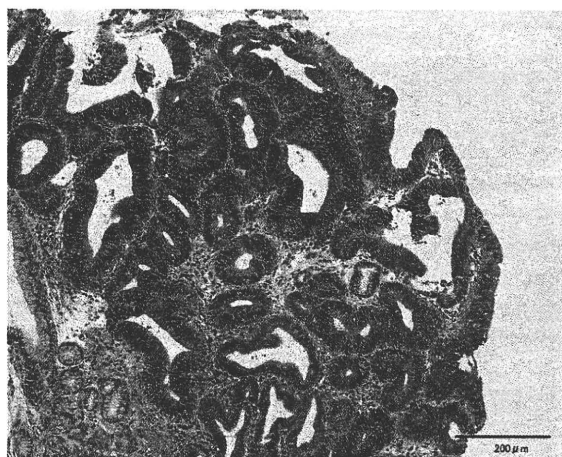
Following the EUS examination, we carried out endoscopic treatment of the minute cancer and esophageal

Figure 1 Minute cancer of the esophagogastric junction. White arrows indicate the minute cancer.

Figure 3 Esophageal varices. (A) The lower esophagus and gastroesophageal junction. (B) The middle esophagus.

varices. The endoscope (GIF-Q200, Olympus Optical Co., Tokyo, Japan) was preloaded with an overtube, which was passed into the oropharynx over the already introduced endoscope. The tip of the endoscope was loaded with a pneumatic EVL device (Sumitomo Bakelite, Tokyo, Japan). Under full endoscopic suction, the minute cancer was tightly packed inside the cap of the endoscope, and the tripwire was pulled, creating an artificial polyp that included the lesion. After confirmation that the electrocautery markings were contained in the ligated band, resection was not performed for the lesion. EVL was successively done for the esophageal varices in three places. All EVL bands were placed in the esophagus and EGJ.

The iatrogenic ulcers in the esophagus and EGJ resulting from the EVL were treated with the administration of a proton pump inhibitor and sodium alginate.

The ulcers were observed endoscopically three months after the procedure to check for the presence of any residual lesion or other lesions, and forceps biopsy specimens were obtained from the site of the resection. A follow-up examination after two years did not show recurrence of the disease (Figure 5).

Figure 2 Histological examination of the biopsy specimen showed well-differentiated adenocarcinoma (hematoxylin and eosin staining, original magnification ×100).
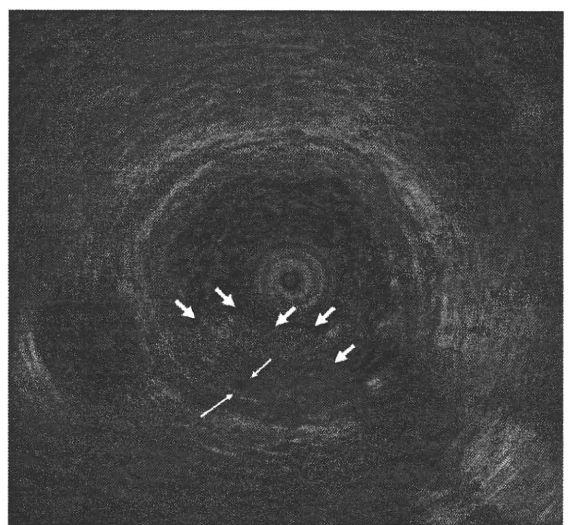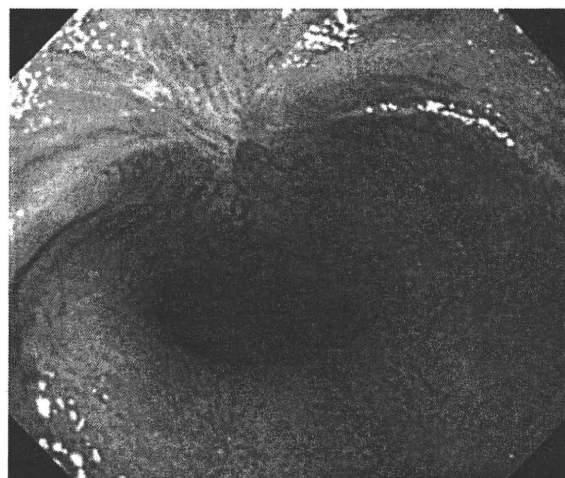

Figure 4 Endoscopic ultrasonography with Olympus UM2000 (Olympus Optical Company, Tokyo, Japan), demonstrates that the minute cancer was noninvasive carcinoma (carcinoma *in situ*) and a 2-mm diameter blood vessel (thin white arrows), feeding the esophageal varices, pierces the lesion. Thick white thick arrows indicate the minute cancer.

Figure 5 Iatrogenic ulcer has healed with scarring, but without any residual lesion.

Discussion

Endoscopic resection has the advantage of providing a full specimen for histological examination and for the diagnosis of the extent and infiltration depth of the lesion. The outcome of endoscopic therapy can therefore be evaluated on the basis of macroscopic and histologic findings. However, in our case, our patient with minute cancer, complicated with esophageal varices, was at a high bleeding risk because of standard endoscopic mucosal resection or endoscopic submucosal dissection. We thus selected endoscopic therapy using EVL, without mucosal resection, for this lesion. This technique had several limitations that may need to be considered. First, large lesions cannot be completely excised with this method because of the size limitation of the friction-fit adaptor. In our case, the diameter of the cancer was less than 10 mm in diameter. Second, because a full specimen cannot be provided, histological examination and the diagnosis of the extent and infiltration depth of the lesion cannot be evaluated.

Conclusion

We believe that because of its technical simplicity and safety, endoscopic therapy using an EVL device for minute cancer of the EGJ, complicated with esophageal varices, may be an acceptable and easily applicable method.

Consent

Written informed consent was obtained from our patient for publication of this case report and any accompanying images. A copy of the written consent is available for review by the Editor-in-Chief of this journal.

Abbreviations

EGJ: esophagogastric junction; EVL: endoscopic variceal ligation; EUS: endoscopic ultrasonography.

Authors' contributions

TA, YA, HT and KY analyzed and interpreted our patient data. HI, HE and KH analyzed endoscopic data. AR, SY and YI performed the histological examination of the organs. TA, MI and AN were major contributors in writing the manuscript. All authors read and approved the final manuscript.

Author Details

[1]Gastroenterology Division, Yokohama City University School of Medicine, Japan and [2]Department of Pathology, Yokohama City University Hospital, Japan

References

1. Iishi H, Tatsuta M, Okuda S: **Endoscopic diagnosis of minute gastric cancer of less than 5 mm in diameter.** *Cancer* 1985, **56**:655-659.
2. Oohara T, Aono G, Ukawa S, Takezoe K, Johjima Y, Kurosaka H, Asakura R, Tohma H: **Clinical diagnosis of minute gastric cancer less than 5 mm in diameter.** *Cancer* 1984, **53**:162-165.
3. Tada M, Murakami A, Karita M, Yanai H, Okita K: **Endoscopic resection of early gastric cancer.** *Endoscopy* 1993, **25**:445-450.